ANNUAL REVIEWS

Annual Review of Earth and Planetary Sciences

The Compositions of Planetary Cores

Anat Shahar,[1] Edward D. Young,[2] Kei Hirose,[3,4] and Shunpei Yokoo[3]

[1]Earth and Planets Laboratory, Carnegie Institution for Science, Washington, DC, USA; email: ashahar@carnegiescience.edu

[2]Department of Earth, Planetary, and Space Sciences, University of California, Los Angeles, USA

[3]Department of Earth and Planetary Science, The University of Tokyo, Tokyo, Japan

[4]Earth-Life Science Institute, Institute of Science Tokyo, Tokyo, Japan

Annu. Rev. Earth Planet. Sci. 2026. 54:559–84

First published as a Review in Advance on February 24, 2026

The *Annual Review of Earth and Planetary Sciences* is online at earth.annualreviews.org

https://doi.org/10.1146/annurev-earth-040722-094945

Keywords

terrestrial planet, metallic core, light element composition, exoplanet

Abstract

Understanding the composition of metallic cores in planetary bodies is crucial for unraveling planetary formation, differentiation, and evolution. On Earth, early seismic and density data suggested iron-dominated interiors alloyed with lighter elements such as sulfur, silicon, oxygen, carbon, hydrogen, and nitrogen. These elements influence core density, thermal conductivity, magnetic field generation, and surface habitability, and their incorporation depends on each planet's unique pressure, temperature, and redox conditions during differentiation. Experimental investigations of metal-silicate partitioning under extreme conditions show that many light elements are strongly siderophile at high pressures, contributing to the diversity of core compositions across the Solar System and beyond. This review synthesizes current knowledge on core compositions beyond Earth—spanning asteroids to exoplanets—and explores how laboratory experiments, cosmochemical evidence, and astrophysical observations collectively inform our understanding of core formation. By decoding core compositions, studies can better constrain the thermal histories and potential habitability of planetary bodies.

- Planetary core compositions reveal how planets form, differentiate, and evolve, shaping the density, heat flow, magnetic fields, and habitability of a planet.

- Experiments, cosmochemical abundances, and theoretical calculations explain the light element compositions of planetary cores from asteroids to exoplanets.

1. INTRODUCTION

The presence and composition of metallic cores in planetary bodies have long presented a fundamental enigma in planetary science (Wiechert 1897). Seismic data from Earth and density estimates of other terrestrial planets have supported the hypothesis that these bodies possess dense, iron-rich interiors. Modern studies, combining high-pressure experiments, cosmochemical constraints, and planetary magnetic field observations, reveal that planetary cores are not composed of pure iron but instead consist of iron alloyed with lighter elements. Variations in these core compositions can have profound implications for a planet's thermal evolution, magnetic field generation, and surface habitability. However, the exact composition remains uncertain, largely due to the challenge of replicating core-forming conditions—pressures of hundreds of gigapascals and temperatures exceeding several thousand kelvin—in laboratory settings. Recent interest in exoplanetary systems has further highlighted this mystery, as researchers seek to infer interior compositions of rocky planets from mass and radius measurements, underscoring the central role of metallic cores in understanding planetary differentiation and evolution across the galaxy.

The composition of the metallic core is dictated by the bulk planet compositions and the physical and chemical conditions of the molten planetary body that then control the partitioning of the elements between the metal and the silicate portion of the planet. The partitioning between liquid iron and silicate melt has been examined under high pressure-temperature (P-T) conditions for a variety of elements, including moderately siderophile (iron-loving) elements, which are present in both mantle and core. The metal-silicate partitioning experiments also demonstrate that the light elements are strongly siderophile under high pressures. As each planet has a unique composition, temperature, pressure, and oxygen fugacity, the resulting cores will have a unique composition. Determining what that composition is can allow scientists to unravel the history of the planet. The most common elements studied as alloying with metallic iron and nickel within planetary cores are hydrogen, carbon, nitrogen, sulfur, silicon, and oxygen. Experimentally, these elements have been shown to alloy with iron at high pressures and temperatures and have been shown to be cosmochemically plentiful. While all these elements are able to alloy with iron, each element has its own unique conditions with which it is more likely to do so, as well as other elements that it avoids or interacts with. As an example, if a planet has a core that is mostly alloyed with sulfur, it will likely have a lower formation temperature than one that is alloyed with silicon. If a core has oxygen and silicon, then it tells us about the oxidation state during core-mantle differentiation. Several excellent reviews have been written about the composition of Earth's core (e.g., Hirose et al. 2021, Fischer & McDonough 2024), so in this review we focus on what is known about the metallic cores of planetary bodies in general, from asteroids to exoplanets.

2. DETERMINING THE COMPOSITION OF PLANETARY CORES

2.1. Cosmochemical Constraints

Geophysics provides direct evidence that Earth's core is not just an Fe–Ni alloy but also includes about 5–10% of lighter elements (Birch 1952). To learn more about which light elements, and more about a planet's overall makeup, we turn to meteorites, which provide indirect evidence of composition. These meteorites provide the basis for models of bulk Earth and primitive mantle, which in turn help to infer what the core is made of. While there is no one meteorite group that can represent the exact composition of bulk Earth or the other terrestrial planets, carbonaceous chondrites provide a reasonable starting point. The CI carbonaceous chondrites have the most primitive composition of all meteorites that also match the composition of the solar photosphere (Anders & Grevesse 1989). Therefore, one way to study the composition of planetary cores is to look at the composition of these chondrites and compare it to the composition of the mantle of a planetary body. Any differences could be due to the sequestration of that element in the core of the planetary body. Elements are siderophile at different pressure and temperature conditions (Thibault & Walter 1995). So depending on the size of the planetary body, the *P-T* conditions during the metal-silicate separation, and the oxidation state of that body, different elements would be predicted to be in the cores. One can also learn about the composition of a planetary core from iron meteorites that represent disrupted cores of planetary bodies. All iron meteorites are made up of an Fe-Ni alloy with other minor minerals and elements. The presence of nickel in all these meteorites is indirect evidence that all planetary cores also contain nickel. In general, the presence of light elements within different iron meteorites is in the form of carbides, sulfides, and trace amounts of nitrogen, silicon, and phosphorous (Scott 2020). Unfortunately, a light element such as hydrogen that could have been present when the core formed would not be detectable today due to diffusion.

2.2. Constraints from Properties of Iron Alloys

Metallic core compositions can be constrained by comparison between high-pressure properties of iron alloys and observations. Such properties include (*a*) density, (*b*) velocity, (*c*) the liquidus field of Fe, (*d*) liquidus temperature (temperature at the onset of Fe crystallization), and (*e*) solid Fe/liquid element partitioning. Studies from Earth-relevant conditions have shown that planetary iron cores most likely include more than one major light impurity element, as a single light element cannot explain the densities of Earth's outer and inner cores (e.g., Miozzi et al. 2020). Further, so many elements are siderophile at these high *P-T* conditions that it is hard to imagine that only one entered the metallic core of the planetesimals. Strong interactions between light elements may cause (*f*) liquid-liquid immiscibility and simultaneous solubility limits, which also help narrow down the range of possible core compositions. Furthermore, the liquid core composition might have been determined by (*g*) metal-silicate chemical equilibration at the time of core formation.

2.2.1. Density and velocity of liquid/solid iron and iron alloys. The pressure-volume-temperature equations of state (EoS) of Fe and Fe alloys have been extensively studied by experiments as well as theoretical calculations, usually combined with synchrotron X-ray diffraction (XRD) measurements (e.g., Pamato et al. 2020). Dynamic compression by shockwave also provides direct density and velocity measurements along the Hugoniot. Such measurements and calculations have been reported for both liquid and solid, and can be applied to examine outer- and inner-core compositions. Any differences in density and velocity between Fe and the outer/inner core are caused by the presence of light elements (e.g., Badro et al. 2007). The candidate light elements of H, C, O, Si, and S reduce the liquid Fe density but increase its P-wave velocity, while heavy nickel has opposite effects. On the other hand, the light elements reduce the P- and S-wave velocities of solid Fe. It is noted that the density of liquid Fe alloy changes with temperature, and therefore the density deficit depends on the core temperature, which is not known. The compressional wave speeds of liquid Fe and Fe alloys are, in contrast, not sensitive to temperature.

Diffuse scattering signals in XRD data, characteristic of liquid, can be used to derive the density of liquid (e.g., Morard et al. 2013). It is, however, challenging because the range of observed diffraction angles is always limited in experiments. Kuwayama et al. (2020) developed a new analytical method to determine the liquid density more precisely than before, which provides a high

P-T liquid Fe density with uncertainty of 1–2%. Shockwave data in the liquid phase along the Hugoniot provide direct liquid density and velocity measurements (Huang et al. 2018), although the shock temperature has to be derived from thermodynamic models. For static compression measurements, the P-wave velocity of liquid Fe was determined by synchrotron inelastic X-ray scattering (IXS) measurements and combined with the density measurements to obtain a good reference to estimate the density deficit and velocity excess of the outer core (Kuwayama et al. 2020).

The high *P-T* densities of liquid Fe and Fe alloys can also be determined by first-principles calculations. Indeed, the experiment-based EoS by Kuwayama et al. (2020) is found to be quite consistent with the theoretical calculations by Vočadlo et al. (2003) and Yokoo et al. (2024). The effects of H, C, O, Si, and S impurities on liquid Fe density have been estimated by Badro et al. (2014) and Umemoto & Hirose (2020). These theoretical calculations showed a smaller effect of a given amount of C or S, and thus required higher concentrations to explain a given density deficit than did experimental results.

The IXS measurements on solids have been made mainly at 300 K, showing the linear relationship between density and P-wave velocity, called Birch's law. Such an empirical law is helpful to extrapolate the density-velocity data to greater than 330 GPa. The effect of temperature on Birch's law has been a matter of debate (Antonangeli et al. 2012, Mao et al. 2012, Sakamaki et al. 2016) but is the key to extrapolating to the conditions of planetary cores. Recent advances of picosecond acoustic measurements in a diamond anvil cell (DAC) also provide the P-wave velocity of solid Fe and Fe alloys at high pressure and room temperature, which is generally consistent with the results of IXS measurements (Decremps et al. 2014, Edmund et al. 2020, Wakamatsu et al. 2022). In addition, shockwave data provide simultaneous high-pressure and -temperature measurements along the Hugoniot that can directly compare with density and velocities under core conditions (Huang et al. 2022).

2.2.2. Liquidus field and temperature. On planets with possible inner and outer cores, the composition of the iron at the liquidus is important for knowing if the light elements partition into the liquid or solid core. This is important for understanding potential magnetic fields on planets, for example. It is known that all of the possible core major light elements form a eutectic system with Fe. Results of melting experiments and extrapolations suggested the binary eutectic liquid compositions at 330 GPa to be Fe containing 1.1 wt% H (Mita et al. 2025), 3.5 wt% C (Mashino et al. 2019), 18.4 wt% O (Sakai et al. 2022), 8.0 wt% Si (Hasegawa et al. 2021), and 7.7 wt% S (Thompson et al. 2022). So theoretically, these are the maximum concentrations of each light element in an outer core that will crystallize a light element–depleted inner solid core.

Liquidus phase relations have also been examined for ternary and quaternary Fe alloy systems at extreme pressure in the laser-heated DAC: Fe-H-O (Oka et al. 2022), Fe-H-Si (Hikosaka et al. 2022), Fe-C-O (Sakai et al. 2022), Fe-C-Si (Hasegawa et al. 2021, Miozzi et al. 2020), Fe-O-S (Yokoo et al. 2019), Fe-Si-S (Tateno et al. 2018), and Fe-C-O-S (Yokoo & Hirose 2024). The limited simultaneous solubilities of Si + O make the examination of the Fe-O-Si liquidus phase diagram difficult (Hirose et al. 2017, Helffrich et al. 2020). With the exception of the Fe-C-Si system, the ternary eutectic liquid composition is located close to the tie line between the two relevant binary eutectic liquid compositions. This means that the liquidus field of Fe in the ternary system is approximately bounded by a mixing of binary eutectic liquid compositions.

Recently Mita et al. (2025) estimated the effect of each light element on the depression of the liquidus temperature of Fe based on a combination of the binary eutectic temperature and composition. When considering the effect of each light element by the amount that causes a specific density depression, the effect is large for C and S and relatively small for H, O, and Si.

2.2.3. Liquid-liquid immiscibility. Liquid-liquid immiscibility is widely observed in liquid Fe–light element systems at ambient pressure due to strong interactions between the light elements. Such nonideal mixing behavior generally diminishes with increasing pressure but is relevant to metallic cores of Mars and other terrestrial bodies smaller than Earth. It may also be important for Earth's core metal segregation processes, in which there might have been a variety of core-forming metals that were enriched in different light elements. The immiscibility between H-rich and S-rich Fe liquids is exceptional; it occurs only above 20 to over 100 GPa (Yokoo et al. 2022). The immiscible Fe-Si and Fe-Si-O liquids were also reported (Arveson et al. 2019).

Limited simultaneous solubility is also caused by strong interactions between light elements. It is known for C and S (Tsuno et al. 2018), C and Si (Li et al. 2015), C and H (Hirose et al. 2019), and O and Si (O'Neill et al. 1998, Hirose et al. 2017, Helffrich et al. 2020).

2.3. Isotopic Constraints

The use of nontraditional stable isotopes to constrain the composition of metallic cores has emerged as a powerful tool in geochemistry and planetary science. Isotope fractionation arises from differences in zero-point vibrational energies of isotopically substituted bonds, as described by quantum mechanical models. The vibrational frequency of a bond, and thus its zero-point energy, is inversely proportional to the reduced mass of the bonded atoms. Heavier isotopes lower the vibrational frequency, stabilizing the bond and driving fractionation at equilibrium. The classic works of Bigeleisen & Mayer (1947) and Urey (1947) showed that the magnitude of equilibrium isotope effects decreases with increasing temperature and atomic mass. The underlying principle hinges on the fact that even at high temperatures, where equilibrium isotope effects are typically minimized, subtle but resolvable fractionation can persist between metal and silicate phases.

With regard to planetary cores, a critical control on high-temperature isotope fractionation is the bonding environment of the metal. As an example, the bonding environment of iron in a silicate will be fundamentally different than the bonding environment of pure iron metal. In silicate phases, the oxidation state of iron, the composition of its coordinating ligands, and its coordination number can all vary, with each contributing to a possible isotope fractionation between a silicate phase and a metal phase. This is also the case for other elements that can be sequestered into a metallic core such as silicon, hydrogen, nitrogen, or oxygen, and even heavier elements such as chromium. If we assume that Earth's starting isotopic composition is similar to that of carbonaceous chondrites and we are able to prove that the bulk silicate Earth does not have the same composition, then it is possible to state that there might have been an isotopic fractionation during an element's sequestration into the core, and therefore the presence of that element within the core (**Figure 1**). The best way to prove this, of course, is to conduct high-pressure and -temperature experiments and determine the isotopic fractionation factors for the system. However, these experiments are not simple, and there has been tremendous disagreement in the literature regarding their accuracy and effectiveness. In particular, it has been made abundantly clear that proving and obtaining equilibrium in such experiments are crucial and not always simple (Shahar et al. 2017).

To date, experiments have been conducted looking at the stable isotopic fractionation during core formation in the silicon, chromium, iron, nitrogen, sulfur, molybdenum, nickel, zinc, ruthenium, and copper systems (e.g., Roskosz et al. 2006; Schuessler et al. 2007; Shahar et al. 2009, 2011; Hin et al. 2012, 2013, 2014; Lazar et al. 2012; Kempl et al. 2013; Bridgestock et al. 2014; Savage et al. 2015; Bonnand et al. 2016; Labidi et al. 2016; Li et al. 2016; Fischer-Gödde & Kleine 2017; Dalou et al. 2019; Elardo et al. 2019). By far, the most studied system is iron. As the main element present in a planetary metallic core, it is the best isotopic system to start understanding isotopic fractionation during differentiation. Further, studies have shown that, in both low- and

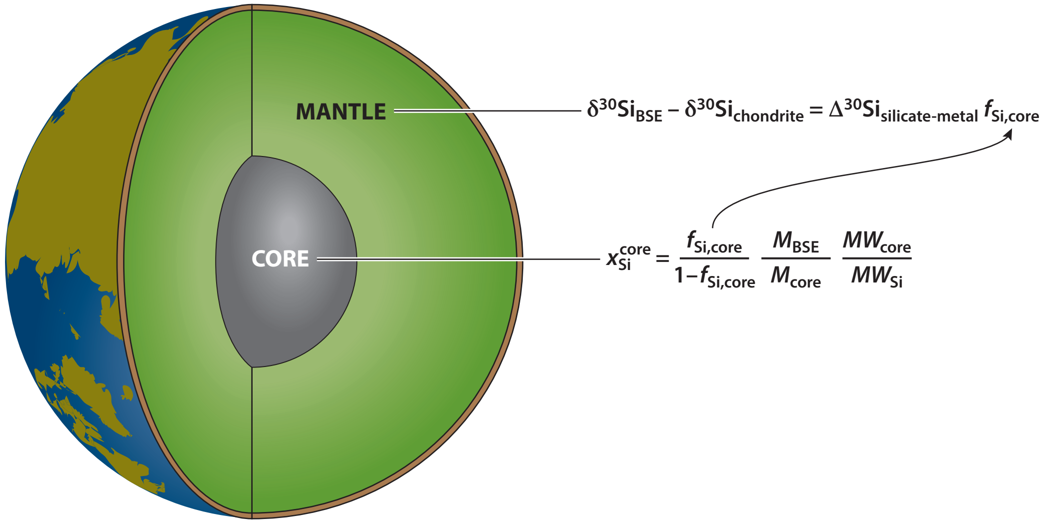

Figure 1

A schematic illustrating, using silicon isotopes as an example, the connection between the difference in silicon isotope ratios ($\delta^{30}Si$) between BSE and chondrite, and the fraction of Si in Earth's core. In the equations, $f_{Si,core}$ is the fraction of Earth's silicon in the core, and x_{Si}^{core} is the mole fraction of Si in metal. Abbreviations: BSE, bulk silicate Earth; M, mass; MW, molar weight. Figure adapted from Young et al. (2015).

high-temperature environments, the oxidation state (Fe^{3+}, Fe^{2+}) exerts strong control on the magnitude of the iron isotope fractionation (Williams et al. 2004, Shahar et al. 2008). Theoretical and experimental results at low temperature have shown that speciation (bond partner and coordination in a solution) also regulates mass fractionation of Fe. In high-temperature solids or melts, the ligand to which Fe is bound also should affect the iron isotopic fractionation (Schauble 2004). Therefore, iron was the best candidate for starting to understand high-temperature isotopic fractionation as not only was iron present in silicates and metals but also the exact composition of the core could be determined by understanding how the isotope fractionation changes depending on the ligand bonded to iron (Shahar et al. 2016). Shahar & Young (2020) review the literature to date on this topic. Most recently, a study has parameterized all the experimental data to date and found that, indeed, there is a small iron isotopic fractionation during core formation, it is very much pressure dependent (size of planet), and it is most evident if there is hydrogen alloyed with iron in the metallic core (Ni et al. 2022).

Work in most other isotopic systems occurs when an element is found to be fractionated relative to chondrite and a mechanism is needed to explain that fractionation. If the element is one where it could be alloyed with iron, then core formation is considered an option. This is the case for the silicon, chromium, nitrogen, sulfur, molybdenum, nickel, ruthenium, and copper systems. This field of inquiry is still young, and there are many isotopic systems to explore. Given the time and effort required for these complex experiments, it is crucial that they are designed to robustly demonstrate equilibrium, ensuring that the resulting data meaningfully advance the field and maintain the integrity of the scientific record.

3. THE SOLAR SYSTEM

3.1. Earth

How do we constrain Earth's core composition? Earth's core likely includes several major light elements (H, C, O, Si, and S), whose concentrations are not really known (Poirier 1994). In order to constrain their abundances, comparing the density and velocity between differing Fe alloys with seismological observations is key. The former is temperature dependent except for the velocity of liquid Fe and Fe alloys; however, the core temperature is also largely unknown. The terrestrial core also includes Ni, whose abundance may be ∼5–10%, but it is difficult to estimate precisely because it least changes the property of Fe. Note also that the chemical compositions of the outer and inner cores are different, but one can be calculated from the other based on the solid Fe–liquid partition coefficients. Overall we have a total of six unknowns to be solved.

How many independent constraints do we have on Earth's core composition and temperature? Seismological observations allow us to constrain the (*a*) density and (*b*) P-wave velocity of the liquid outer core and the (*c*) density and (*d*) P-wave and (*e*) S-wave velocities of the solid inner core. Because of vigorous convection required to generate the planetary magnetic field, the liquid core may be well-mixed possibly except at its top and bottom few hundred kilometers (called E′ and F layers, respectively, both exhibiting slow P-wave velocities). Even if there is no convection in the inner core (Gomi & Hirose 2023), the compositional gradient in the inner core should be small when considering that it crystallizes from a liquid core and constitutes only 5% by weight of the entire core. The presence of the inner core by itself is an important constraint on the composition and temperature of the outer core; the outer-core liquid composition must be within (*f*) the liquidus field of Fe (on the Fe side of any eutectic points or cotectic lines), and (*g*) the liquidus temperature of the outer-core liquid at 330 GPa corresponds to the temperature at the inner-core boundary (ICB). In addition, (*h*) solubility limits, in particular Si + O, can be important. (*i*) Metal-silicate partitioning of light elements might be helpful, although their incorporation into the core strongly depends on core formation processes, which must have been more complex than usually assumed. Finally, (*j*) cosmochemical constraints suggest ∼2 wt% S in Earth's core (Dreibus & Palme 1996), considering its mantle and bulk Earth abundances. Overall, we can constrain the range of possible core compositions by using these total ten independent constraints on the six unknowns.

3.1.1. Estimate of Earth's core temperature. Once we know the core temperature at one place, for example at ICB, we can calculate adiabatic temperature profile using the density profile from a seismological model and Grüneisen parameter that is a function of pressure, temperature, and composition but is assumed to be constant at 1.5 along the core *P*-*T* profile (Vočadlo et al. 2003):

$$T = T_X \left(\frac{\rho}{\rho_X}\right)^{\gamma}, \tag{1.}$$

leading to $T_{ICB} = 1.36 \times T_{CMB}$. It has been argued that the core-mantle boundary (CMB) temperature is lower than the solidus temperature of the mantle because otherwise the bottom of the mantle would be globally molten. The ultra-low-velocity zones above the CMB may represent partially molten areas but are observed only locally, suggesting that they are attributed to melting of materials with relatively low melting temperatures such as FeO-rich ones (note that the ternary minimum on the liquidus surface of the SiO_2-MgO-FeO system is located close to the FeO end-member) (Boukaré et al. 2015, Helffrich et al. 2020). It is therefore likely that the CMB temperature is lower than the pyrolite solidus at that depth, which has been determined to be ≈4,100 (Fiquet et al. 2010, Andrault et al. 2011) or ≈3,600 K (Nomura et al. 2014, Kim et al. 2020). The CMB temperatures of 4,000 and 3,500 K give 5,400 and 4,780 K at the ICB, respectively. Li et al. (2018) argued that the temperature at 360 GPa near Earth's center is higher than 5,500 K to reconcile the observed density and velocity of the inner core with Fe-C-Si-S alloys when considering the melting temperature. Because the ICB temperature could be lower by at

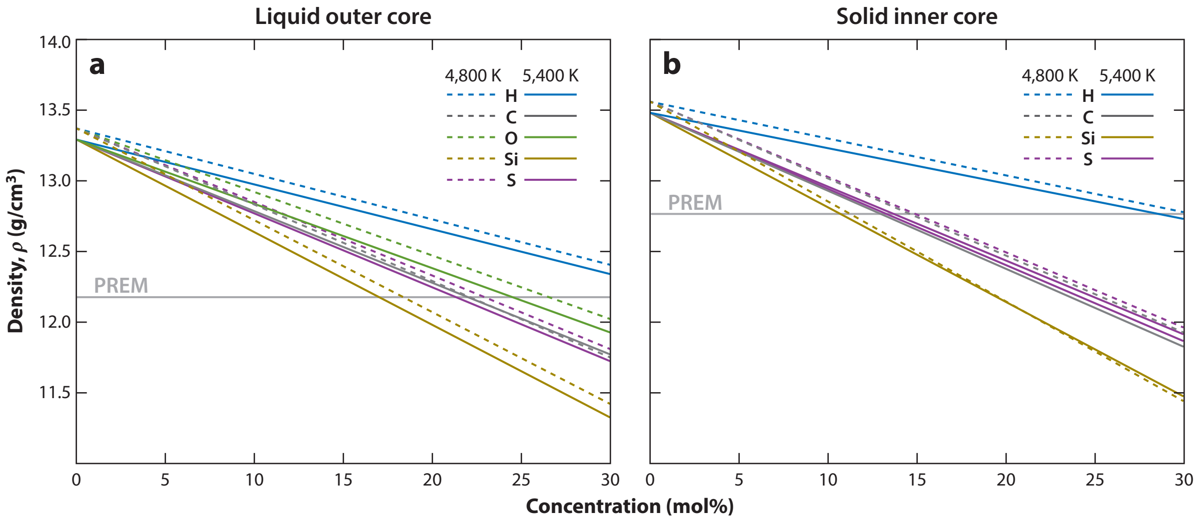

Figure 2

Reductions in density due to incorporation of each light element into Fe at the inner-core boundary pressure of 330 GPa and 5,400 K (*solid lines*) and 4,800 K (*dotted lines*) for (*a*) the liquid outer core and (*b*) the solid inner core of Earth. Abbreviation: PREM, preliminary reference Earth model.

most a few hundred degrees from the center, their estimate is marginally consistent with $T_{\mathrm{ICB}} =$ 4,800 to 5,400 K.

The ICB temperature is given as the liquidus temperature of the outer-core liquid. As described above, the effect of each light element on the depression of the liquidus temperature of Fe has been estimated based on a combination of the binary eutectic temperature and composition at 330 GPa (Mita et al. 2025). It is useful to match the liquidus temperatures of possible outer-core liquid compositions with $T_{\mathrm{ICB}} =$ 4,800 to 5,400 K. We have to note, however, that such estimates of liquidus temperatures assume that the additive effects of each light element differ from experimental data up to about 10%. Moreover, Mita et al. (2025) used 6,230 K for the melting temperature of pure Fe at 330 GPa from Anzellini et al. (2013), which is relatively high.

3.1.2. Constraints from seismological observations. The density and P-wave velocity of liquid Fe alloys have been calculated from theory in the Fe-C-O-Si-S system assuming $T_{\mathrm{ICB}} =$ 6,300 K by Badro et al. (2014) and in the Fe-H-C-O-Si-S system at $T_{\mathrm{ICB}} =$ 4,800 to 6,000 K by Umemoto & Hirose (2020). Considering the ICB temperature is possibly between 4,800 and 5,400 K, the latter calculations indicate that the seismological observations of the outer-core density and P-wave velocity can be explained (**Figure 2**), considering both observational and theoretical uncertainties, by liquid Fe containing 0.96–1.12% H, 8.4–9.9% O, 9.3–10.4% Si, or 13.3–15.0% S by weight when the core includes a single light element (carbon alone cannot explain these observations). Because the density and P-wave velocity of a liquid Fe containing multiple light elements are well-reproduced by mixing of binary alloy liquids under core high *P-T* (Umemoto & Hirose 2020), the outer-core composition is possibly a mixture of these four end-member liquids with a minor amount of C.

It has been reported that the S-wave velocity of the inner core is much lower than that of pure Fe; the observed P- and S-wave velocities are lower by 10% and 30%, respectively, than those of solid pure Fe at 360 GPa and 5,000 K (Li et al. 2018). Recent measurements of the S-wave velocity of Fe-Si alloy by shockwave showed that incorporation of Si in the inner core would not be sufficient to explain the observed low S-wave velocity (Huang et al. 2022). It may require large amounts of C (Li et al. 2018) and/or H (Wang et al. 2021), although the former is not feasible because of the low solid Fe/liquid partition coefficient of C. The most recent calculations by Gomi & Hirose (2025) found that the depth versus bulk sound velocity profile in the inner core given by the preliminary reference Earth model and AK135 models exhibits a much smaller gradient than any of the 693 different calculated Fe-Ni-Si-S-H alloys, possibly implying a strong compositional gradient far more than expected during 5% crystallization of the liquid core. Alternatively, it might suggest that the inner-core shear velocity is not well-represented by these reference seismological models (Dziewonski & Anderson 1981, Montagner & Kennett 1996).

3.1.3. Possible range of Earth's liquid core composition. Here we estimate the possible range of Earth's liquid core composition based on many of the constraints described above. Employing (*a*) T_{ICB} = 4,800–5,400 K, (*b*) the liquidus temperature of Fe alloys, (*c*) outer-core density and velocity, (*d*) inner-core density, and (*e*) Si + O solubility limit, the outer-core liquid may include 0.1–0.7 wt% H, 0–0.5 wt% C, 0–2 wt% O, and 2–6 wt% Si in addition to 1.7 wt% S (assumed by following Dreibus & Palme 1996) when 10% uncertainties in estimates of the liquidus temperatures of iron alloys are considered. This gives 0.1–0.6 wt% H, <0.1 wt% C, 2–6 wt% Si, and 0–0.8 wt% S (practically no oxygen) in the inner core based on solid Fe/liquid partition coefficients of these light elements (Oka et al. 2022, Sakai et al. 2023).

As discussed above, the liquidus field of Fe may be approximated by mixing each binary eutectic liquid composition in the Fe-H-C-O-Si-S system. The possible liquid core compositions mentioned above are not within such a mixing field but are located 10–20% outside of it. Nevertheless, it is still feasible for such liquids to crystallize Fe; indeed, the liquidus field of Fe must be wider than the field defined by mixing each binary eutectic liquid. Such a core composition has far-reaching implications for Earth's accretion and core formation processes. The Mg/Si molar ratio of Earth's upper mantle is 1.3, significantly higher than those of chondritic and solar compositions (1.0). The approximate 4 wt% Si in the core explains the "missing Si" problem (Allègre et al. 2001, Dauphas et al. 2015). Up to 0.7 wt% H and 0.5 wt% C in the core suggest that most of the bulk Earth H and C budgets could be present in the core. Enrichment in H supports that several tens of ocean mass of water might have been delivered to the growing Earth (Tagawa et al. 2021, Young et al. 2023).

3.2. Mars, Mercury, and Venus

3.2.1. Mars. The understanding of the state and composition of Mars's core has been greatly improved by the Interior Exploration using Seismic Investigations, Geodesy and Heat Transport (InSight) mission, recently conducted by NASA. Seismic waves that reflected from the solid-liquid boundary in the deep interior of Mars were first reported, and the radius of the molten core (∼1,730–1,870 km) was found to be larger than previously thought if all of this liquid region represents the core (Stähler et al. 2021, Drilleau et al. 2022, Durán et al. 2022, Irving et al. 2023). The large core supports the relatively low average density of the core of 5.7–6.35 g/cm^3. The detection of the solid-liquid boundary by seismological observations is consistent with a (at least partially) molten core as suggested by the solar tidal deformation (Yoder et al. 2003) and nutation amplitudes (Le Maistre et al. 2023). In addition to reflections from the boundary, Irving et al. (2023) reported waves that transit through the liquid core. The absence of the solid inner core on the paths of such core-transiting waves does not exclude the possible presence of the solid inner core but constrains its maximum radius to be 750 km. More recently, Samuel et al. (2023) and Khan et al. (2023) challenged the earlier interpretation that the reflected waves are signals of the CMB. They both proposed a molten silicate layer with a thickness of approximately 150 km at the bottom of the mantle, leading to a smaller core size. Modeled with the molten silicate layer, the radius and average density of the core were revised to be 1,630–1,705 km and 6.41–6.75 g/cm^3, respectively. Importantly, the two studies determined different core properties for Mars, as the Samuel et al. (2023) paper used only experimental data to determine the EoS and the properties (and hence composition) of the Martian core, while the Khan et al. (2023) paper used ab initio simulations, which are not reliable in this context due to their treatment of the magnetic properties of the alloys.

The average density of the core, which is less dense than liquid pure Fe (Kuwayama et al. 2020), constrains the abundance of light elements in the core. Based on the liquid densities of Fe–light element binary alloys (Kawaguchi et al. 2022, Huang et al. 2023), the low- and high-density estimations (without and with the molten silicate layer, respectively) correspond to about 36–50 mol% S (24.4–36.5 wt% S) and about 26–36 mol% S (16.8–24.4 wt% S), respectively (**Figure 3**). While sulfur has been widely accepted as an important light element in the core of Mars, its large density deficit suggests the additional presence of other light elements such as oxygen, carbon, and hydrogen (silicon concentration is likely negligible because of oxidizing conditions at the time of core formation, suggested from a high FeO content in the Martian mantle). If a single additional element contributes half of the observed density deficit, it requires 20–30 mol% O (6.7–10.9 wt% O), 37–53 mol% C (11.2–19.5 wt% C), and 41–57 mol% H (1.2–2.3 wt% H) for the relatively

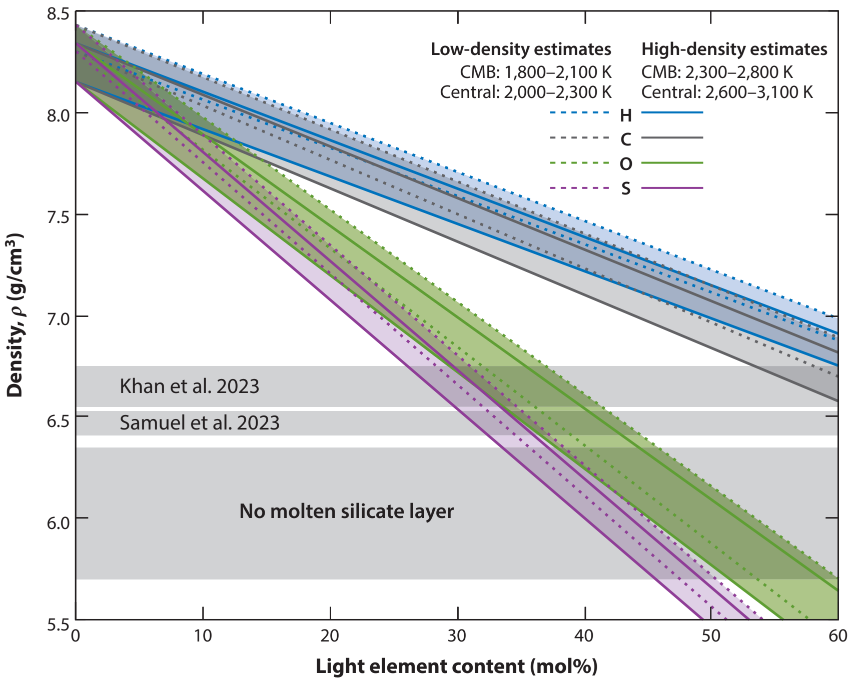

Figure 3

Changes in the average density of the core as a function of light element content (mol%). Solid lines indicate the upper and lower bounds for the high-density estimates assuming the CMB temperature of 2,300–2,800 K and the central temperature of 2,600–3,100 K. Dotted lines indicate those for the low-density estimates assuming the CMB temperature of 1,800–2,100 K and the central temperature of 2,000–2,300 K. Estimates from Samuel et al. (2023) and Khan et al. (2023) and those without the molten silicate layer are shown by gray bands. Abbreviation: CMB, core-mantle boundary.

low-density estimates, and 15–21 mol% O (4.8–7.1 wt% O), 27–38 mol% C (7.4–11.6 wt% C), and 30–41 mol% H (0.8–1.2 wt% H) for the high-density estimates (Morard & Katsura 2010, Komabayashi 2014, Huang et al. 2023, Yokoo & Hirose 2024) (**Figure 3**).

Core formation models have been constructed for Mars (Righter & Chabot 2011, Rai & Van Westrenen 2013, Brennan et al. 2020). Sulfur is strongly siderophile under the core-forming conditions of Mars, and the sulfur content in Mars's core could be as much as 20 wt%, depending on its bulk Mars abundance (Steenstra & Van Westrenen 2018, Brennan et al. 2020). On the other hand, if the bulk Mars sulfur concentration is estimated from chondritic abundance considering its volatility, the mantle sulfur content yields less than 9 wt% S in the core (Yoshizaki & McDonough 2020). The oxygen content in Mars's core estimated from its partitioning behavior is limited to less than 1–4 wt% (Steenstra & Van Westrenen 2018, Brennan et al. 2020). More oxygen may be partitioned into the core if the Martian core metal segregation occurred at higher temperatures (Tsuno et al. 2011). While the carbon content in the core is not well-constrained due to uncertainty in its bulk Mars abundance, its estimate extends to several weight percent. The upper bound of the core carbon content may be given by its solubility in liquid Fe-S, which decreases with increasing sulfur concentration (Tsuno et al. 2018). There are mixed reports of hydrogen in the Martian core, as while it is highly siderophile under high pressure (Tagawa et al. 2021), it has been shown that Mars was likely too small to acquire a hydrogen-rich atmosphere while still molten (Young et al. 2023).

The structure of the Martian core has been discussed based on the Fe-S and Fe-S-(H, C, and/or O) phase relations. The low density of the core indicates the importance of the S-rich side of the Fe-FeS phase diagram. Fe_3S, Fe_2S, $Fe_{3+X}S_2$, and $Fe_{4+X}S_3$ have been reported as Fe-S compounds stable under the Martian core pressure range, although $Fe_{3+X}S_2$ and $Fe_{4+X}S_3$ may represent the same crystal structure (Fei et al. 2000, Oka et al. 2022, Man et al. 2025). Fe and Fe_3S form a eutectic system, and the liquidus phase is Fe_3S for a liquid with 14–16 wt% S and $Fe_{4+X}S_3$ (or $Fe_{3+X}S_2$) for liquid with more than 16 wt% S at 40 GPa (Fei et al. 2000, Stewart et al. 2007, Man et al. 2025). Crystallization of Fe_2S from liquids with 14–16 wt% S is a possibility but has not been investigated yet. The liquidus phase relations of Fe-S-O ternary alloys show the wide liquidus field of FeO (a compositional range from which FeO first crystallizes) compared to those of Fe and Fe sulfide, and liquids with 0.5–2 wt% O and more than 7 wt% S coexist with solid FeO (Tsuno & Ohtani 2009, Yokoo & Hirose 2024). Similarly, the liquidus field of Fe_3C is wide in the Fe-S-C system, and liquids containing 0.5–1.5 wt% C and more than 11 wt% S crystallize Fe_3C (Yokoo & Hirose 2024).

Previously, the crystallization regime of the Martian core had been discussed based on the Fe-FeS binary phase relations (Stewart et al. 2007). According to the light elements–rich compositions obtained from the InSight mission reports, possible inner-core phases are $Fe_{4+X}S_3$ for the S-rich core, FeO for the O-rich core, and Fe_3C for the C-rich core (Yokoo & Hirose 2024, Man et al. 2025) (**Figure 4**). However, because the liquidus temperatures of S-rich liquids are relatively low, the crystallization of $Fe_{4+X}S_3$, FeO, or Fe_3C from liquids containing more than 16 wt% S requires the core cooling to about 2,000 K at the center, which is lower than the recent areotherm estimations (Khan et al. 2023, Samuel et al. 2023). In the case of an H-rich core, when the core cools down to temperatures lower than the miscible-immiscible boundary, the liquid core separates into an H-rich layer and an S-rich layer (Yokoo et al. 2022) (**Figure 4**). The snowing core regime, where solid iron crystallizes at the shallow part of the liquid core and sinks to the deeper part, was once proposed to be a possible crystallization regime (Stewart et al. 2007). However, the sulfur content for the snowing core regime (10–14 wt% S) by itself is smaller than that required to explain the average density of the core, and therefore additional light elements must be included. Because the liquidus phase changes from Fe to a light element–rich phase such as FeO or Fe_3C

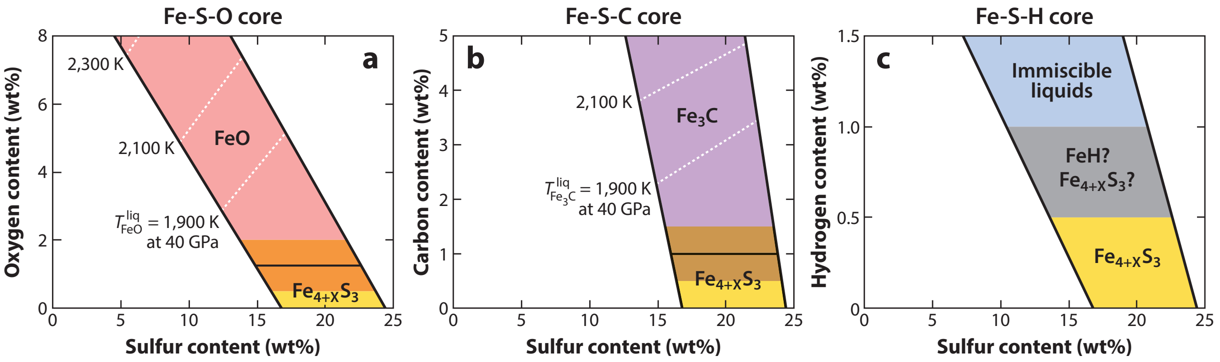

Figure 4

First crystallizing solid phases from the (*a*) Fe-S-O, (*b*) Fe-S-C, and (*c*) Fe-S-H cores, whose compositions are consistent with the high-density estimates (Khan et al. 2023, Samuel et al. 2023). Liquidus temperatures to crystallize (*a*) FeO and (*b*) Fe_3C at 40 GPa are shown by dashed lines (Yokoo & Hirose 2024). Separation into two immiscible liquids occurs at higher temperatures than the crystallization of a solid phase in the (*c*) H-rich Fe-S-H core.

by the addition of small amounts (0.5 wt%) of oxygen or carbon to the liquid, the snowing core is unlikely to occur in the Martian core.

3.2.2. Mercury. Mercury's core is characterized by its large size (2,000-km radius) compared to the bulk planet (e.g., Hauck et al. 2013, Rivoldini & Van Hoolst 2013). It is at least partially molten, which was confirmed by the observations of longitudinal librations and moments of inertia (Margot et al. 2007). Geodetic observations by the MErcury Surface, Space ENvironment, GEochemistry, and Ranging (MESSENGER) spacecraft suggest the existence of the solid inner core, whose radius may be 30–70% of that of the entire core (Genova et al. 2019). In addition to these geodetic properties, spacecraft missions have revealed that the magnetic field of Mercury is active, albeit weak and offset to the north by 400 km (Soderlund et al. 2025). Christensen (2006) demonstrated that stratification at the shallow part of the core and convection only at the deeper part of the core can explain Mercury's magnetic field.

The existence of the liquid core and the active magnetic field, despite the rapid cooling expected from its relatively small size, suggest that Mercury's core also contains light elements that lower the crystallizing temperature of the liquid core. Sulfur is considered one of the major light elements in the Mercurial core because of the low liquidus temperatures of Fe-S alloys (e.g., Chen et al. 2008). Mercury may indeed be S rich, as the surface measurements by the MESSENGER spacecraft obtained the S-rich crustal compositions (Nittler et al. 2011). Silicon is also suggested as the major light element from the surface composition. Low FeO abundance on the surface indicates the reducing conditions of Mercury's core formation (Nittler et al. 2011), under which silicon exhibits a siderophile nature (Corgne et al. 2008). Interestingly, Mercury's surface is enriched in graphite (Peplowski et al. 2016, Lark et al. 2023), implying that carbon is also a candidate light element in the core, although the amount of graphite on the surface is still controversial (Y. Xu et al. 2024).

The silicon content in the core is estimated to be 4.5–21 wt%, depending on the bulk Mercury composition, based on single-stage core formation models that do not consider the presence of sulfur (Steenstra & Van Westrenen 2020). The core carbon content depends on the core silicon content due to the low solubility of carbon in Si-rich liquid iron (Takahashi et al. 2013, Vander Kaaden et al. 2020). The saturation of carbon in Si-rich liquid metal during core formation, as well as in the magma ocean, allows the formation of a graphitic crust, which may be the reason for Mercury's C-rich surface (Vander Kaaden & McCubbin 2015, Steenstra & Van Westrenen

2020). Sulfur is a chalcophile and siderophile element. However, sulfur becomes lithophile (the metal-silicate partition coefficient is less than 1) under reducing conditions (e.g., Rose-Weston et al. 2009). Based on the metal-silicate partitioning experiments simultaneous for sulfur and silicon by Chabot et al. (2014), Mercury's core must contain silicon to explain the high sulfur content in the mantle, and the sulfur content in the core decreases with increasing the silicon content.

Fe-rich face-centered cubic or body-centered cubic alloy crystallizes from a liquid with less than 12 wt% Si (Fischer et al. 2015, Edmund et al. 2022), with negligible differentiation of silicon between solid and liquid (Morard et al. 2014). Si-rich B2 alloy is a crystallizing phase from a more Si-rich liquid and forms a dense inner core if the difference in silicon content between solid and liquid is small enough (Yokoo et al. 2023). Si-rich B20 alloy crystallizes from a liquid with more than 20–30 wt% Si (Kuwayama & Hirose 2004, Edmund et al. 2022), but the pressure range of its stability is limited to a relatively shallow part (<30 GPa) in Mercury's core (Geballe & Jeanloz 2014).

If the core is enriched in both sulfur and silicon, the liquid core could be stratified. Because Fe-S and Fe-Si liquids are immiscible at pressures less than 14 GPa (Sanloup & Fei 2004, Morard & Katsura 2010), the Fe-S liquid outer shell may be formed at the shallow part of the core (Malavergne et al. 2010). Such an Fe-S layer could have formed a solid Fe-S layer at the top of the core, which could explain the high average density of solid layers above the liquid core (Smith et al. 2012). Because the Fe-S and Fe-Si liquids are miscible in the deep Mercurial core, there may be a liquid Fe-Si-S layer below the immiscible layer(s) and above the solid inner core (Malavergne et al. 2010). In such a case, the solid/liquid partition coefficient of silicon increases to more than unity (more silicon is partitioned into a solid) because of the effect of sulfur, while sulfur remains in the liquid (Tao & Fei 2021). In the Si- and C-rich core, the crystallization of the C-poor Fe-Si inner core leads to an increase in carbon content in the liquid core, resulting in a C-saturated condition. This, in turn, may cause diamond crystallization and form a diamond layer at the CMB (R. Xu et al. 2024). Note that the presence of carbon in a liquid enhances the solid/liquid partition coefficient of silicon to more than unity (Hasegawa et al. 2021). The progressive depletion of silicon in the liquid core by the crystallization of the Si-rich inner core increases the solubility of carbon in liquid Fe, which might prevent diamond crystallization.

3.2.3. Venus. The composition and structure of Venus's core are hardly constrained. The radius of the core has been estimated to be 3,500 km with a large uncertainty of more than 500 km based on the moment of inertia (Margot et al. 2021), and it depends on whether the solid inner core exists or not (O'Neill 2021). The absence of the magnetic field indicates that the core does not undergo convection at least at present, despite the planet's size being similar to that of Earth. This may be explained by small heat flux through the CMB and high core temperature due to the slow cooling of the mantle in the stagnant lid regime (Smrekar et al. 2018). The composition of the Venusian core has been proposed based on comparisons with the core compositions of Earth and Mercury, as well as the single-stage core formation model (Trønnes et al. 2019, Shah et al. 2022). In either approach, the FeO content in the mantle is a crucial parameter, and it is desirable to obtain the mantle composition of Venus in future missions.

3.3. Asteroid (16) Psyche

Outside of the terrestrial planets discussed above, there are many other planetary bodies within our Solar System that could add to our understanding of the composition of planetary cores. Unfortunately, to date little is known about many of these bodies. The gas giants—Jupiter, Saturn, Uranus, and Neptune—were long believed to have heavy element cores surrounded by high-pressure hydrogen and helium (Mizuno 1980). However, recent studies using data from Juno and Cassini show that the interiors are much more complex and also very unlike the interiors of terrestrial planets (Militzer et al. 2022, Helled & Stevenson 2024) with less gradient among the layers. For the icy moons (e.g., Ganymede, Callisto, Io, Titan, Enceladus), their interior structures are complicated by below-surface oceans and thick layers of ice (Schubert et al. 2009). Interestingly, a recent study suggests that the interior temperatures of the icy moons might not have ever exceeded the metal-silicate differentiation temperature (Petricca et al. 2025), so the interiors would be very different than those in our terrestrial planets.

However, one unexplored planetary body shows great promise for understanding metallic core compositions within our Solar System: asteroid (16) Psyche, a metal-rich world. In the years to come, more will be learned, as there is currently a NASA spacecraft heading toward Psyche. Measuring the composition of the metallic portion of the largest *M*-type asteroid would be a huge achievement in the quest for direct evidence of the composition of a core. Recent spectroscopic evidence suggests that the asteroid is 30–55 vol% metallic, so not entirely metallic, but with significant amounts (Dibb et al. 2023). The latest density measurement, however, shows a bulk density of $4{,}172 \pm 145$ kg/m^3 (Farnocchia et al. 2024), which is similar to an *M*-type asteroid and makes Psyche the most dense known asteroid. This value gives a wider possible range of metal fractions for the whole body, while it is thought that the asteroid also has silicate components (a more rocky component). The Psyche mission will study the asteroid's composition, topography, and geology. The composition determined will speak volumes to the formation and evolution of this particular asteroid, as well as planetary bodies in general. Several papers have been written explaining how the data will be determined and analyzed (e.g., Elkins-Tanton et al. 2020, Dibb et al. 2023), but for the scope of this review, we focus on what is (un)known about the possible light element composition of the metallic portion.

Thermal emission data from the Atacama Large Millimeter Array suggested that the metallic portion of the asteroid could be consistent with sulfides (de Kleer et al. 2021). With limited data to date, there are a few possible scenarios for the composition of Psyche and the visibility of sulfides. If the asteroid is similar to a carbonaceous Bencubbin-like chondrite, it would have never melted and the sulfides could be evidence of equilibrium condensation or some sort of secondary product of aqueous alteration on Psyche. The other option is that Psyche is a differentiated object that has regions of metal and regions of silicate within a porous body (Elkins-Tanton et al. 2022). For reasons outlined by Elkins-Tanton et al. (2022), it is thought that Psyche is unlikely to be an inner Solar System body and therefore made of noncarbonaceous materials. This is backed up by the inferred small amounts of iron in the silicate portion of the body. A highly reducing environment would account for a low iron content in the silicate as well as the presence of iron metal. If that is in fact the case for Psyche, then the presence of sulfides would point to the presence of other light elements present in the metallic portion of Psyche that were not miscible with the sulfide. Experiments have shown that at lower pressure (below approximately 3 GPa), a metallic iron core with both carbon and sulfur would form two separate liquids. In this case, one would expect that the metallic portion of Psyche might have carbon present. The other option is silicon, which would explain the low iron content of the metal, similar to what is expected on Mercury (Tao & Fei 2021). Silicon enters iron metal at highly reducing conditions, and if sulfur is also present, it will also form two immiscible liquids at low pressure but will close at pressures above 10 GPa. However, upon crystallization, a silicon-iron alloy and a sulfide will be present (Sanloup & Fei 2004), as discussed in more detail in the Mercury section. The presence of carbon or silicon in the metal would point to very different formation conditions for the parent body. The exact composition of the metallic portion of Psyche will help determine the pressure of differentiation of the planetary body, whether it experienced a hit-and-run collision, and if indeed it is a differentiated body.

4. EXOPLANETS

4.1. Bulk Compositions of Exoplanets

In order to evaluate the propensity of extrasolar rocky planets to have metal cores, we must first determine whether their bulk compositions are consistent with having an iron-rich metal core. There are at least three ways to assess this. One is the bulk density of exoplanets as manifested by their masses and radii, where the former come from radial velocity measurements and the latter from transit observations. This method is fraught with uncertainties and degeneracies. Nonetheless, the bulk densities of rock-rich planets can be used to determine their bulk Fe/Mg ratios (Unterborn et al. 2023), and a notional metal core fraction can be estimated from the Fe/Mg ratios regardless of whether such a core really exists or not. These estimates are generally consistent with metal core fractions of about 20–60%. A few planets are overdense as compared to predictions from their stellar hosts, comprising the so-called super-Mercuries. If these bodies form by stripping of silicate mantles due to collisions, their mere existence would be evidence that extrasolar metal-rich cores do indeed form by differentiation in low-mass, rocky planets.

In the most favorable circumstances, mass-radius relationships for rock-dominated planets can yield constraints on the compositions of metal cores, assuming they are present. For example, the seven TRAPPIST-1 planets with masses ranging from 0.33 to 1.32 $M_{\oplus}$ are under-dense relative to Earth (Agol et al. 2021). The low densities have been explained as being due to low-mass fractions of metal cores or as the result of water-rich surfaces (Agol et al. 2021). An alternative is that core fractions are similar to that of Earth but the metal cores have density deficits relative to pure Fe metal of 28–40% (Schlichting & Young 2022).

The second method for estimating the compositions of rocky planets is the link between the relative abundances of rock-forming elements in stellar hosts and those in their orbiting planets (e.g., Hinkel & Young 2025). This correlation permits a comparison of rocky planet bulk densities and the metal mass fractions indicated by the abundances of Fe, Mg, and Si in the host stars (Adibekyan et al. 2021). Results show a correlation between low-mass planet bulk density and estimated iron-rich metal fraction, with typical inferred mass fractions of metal cores of rocky exoplanets in the range of roughly 25–35% (Adibekyan et al. 2021).

Using the Hypatia catalog of stellar abundances for stars within 500 pc of the Sun (Hinkel et al. 2014), Trierweiler et al. (2023) showed that stellar abundances of rock-forming elements of about 70% of stars in the solar neighborhood are consistent with broadly chondritic compositions. These authors also found that the mass fractions of iron metal cores indicated by these abundances have a distinct mode at 32% (i.e., Earth-like) with a 1σ spread of about $\pm$5%. Trierweiler et al. (2023) also found a correlation with overall metallicity, with lower fractions of Fe relative to lithophile elements for those stars formed in the first several billion years of the Milky Way. The calculated iron metal fraction for planets that would have formed around these oldest stars is 20 $\pm$ 5%. Galactic chemical evolution of the elements has resulted in an increase in the metal core fractions of rocky planets with time in the Milky Way.

The third means of determining whether rocky exoplanets have compositions suitable for iron-rich metal cores is through the study of polluted white dwarf (WD) stars. WDs are typically about half the mass of the Sun but only the size of Earth. Due to their immense gravity, rock-forming elements should settle through their hydrogen and/or helium outer envelopes into the depths of these stellar remnants where they are rendered undetectable. Where these elements are detected spectroscopically, they must be exogenous, having been delivered by accretion of rocks and ices similar in mass to the more massive asteroids in the Solar System (e.g., Jura et al. 2007, Zuckerman et al. 2007, Farihi et al. 2010, Gänsicke et al. 2012, Jura & Young 2014, Zuckerman & Young 2018). The iron concentrations in silicate-dominated accreted materials indicate that they have intrinsic oxygen fugacities similar to planetary building blocks in the Solar System (Doyle et al. 2019). This in turn suggests that the planets built from these materials could have Earth-like iron-rich metal fractions (Trierweiler et al. 2023). This observation validates the assumption that the mass fraction of iron determined from stellar abundances is, to first order, equivalent to the mass fraction of an Fe-rich metal core. The advantage of these observations is that they are direct in the sense that the elemental ratios represent actual rocks, as opposed to the host star. The disadvantage is that the uncertainties in element ratios derived from polluted WDs are limiting. However, polluted WD compositions are generally consistent with metal core mass fractions similar to that of Earth, with medians of 25–35% depending on assumptions about settling, with uncertainties ranging from 5% to 15% (Trierweiler et al. 2023).

There is also some more direct observational evidence for rock-metal differentiation for a body orbiting around a WD. Manser et al. (2019) reported periodic shifts in emission spectral lines from an accretion disk around a WD that they argued is best explained by a remnant metal core of a differentiated planetesimal orbiting within the disk around the WD. The metal-like density of the spherical body would explain how it has avoided tidal disruption as it orbits so close to the WD.

4.2. Differentiation

Despite the evidence for Earth-like bulk compositions among extrasolar planetary materials, the familiar concept of a planetary core resulting from silicate-metal differentiation must be scrutinized when applied to extrasolar planets more massive than Earth. Indeed, it is not at all clear that discrete cores of iron-rich metal, alloyed with Ni and various light elements, even exist among the most common type of planets with rock-like interiors. It is reasonable to ask what the likelihood is for Earth-like metal cores among the most common types of rocky exoplanets. In this context, we refer to "cores" in the broadest sense as being everything interior to the atmospheres, or supercritical envelopes of subgiant planets. We use the modifiers "metal" and "silicate" to refer to the specific material comprising the cores.

Based on observations to date, the most common types of extrasolar planets in the Galaxy are the super-Earths and sub-Neptunes (e.g., Fressin et al. 2013). Super-Earths have radii greater than that of Earth but less than about 1.8 $R_{\oplus}$, while sub-Neptunes have radii of between about 2.0 and 4.0 $R_{\oplus}$. The bulk densities of super-Earths indicate that they are rocky planets with broadly Earth-like bulk densities and negligible atmospheres in terms of mass. The compositions of sub-Neptunes are less straightforward in that their bulk densities are open to interpretation. Although some interpretations of sub-Neptune bulk mass–radius relationships have posited that these planets may be a mix of subequal fractions of rock and water (e.g., Zeng et al. 2019), the emerging consensus is that sub-Neptunes likely have rock-like interiors, very likely molten (e.g., Kite et al. 2019, Schlichting & Young 2022, Seo et al. 2024), overlain by substantial primary atmospheres of H/He, also referred to as their envelopes. In order to match the bulk densities of these planets, the envelopes must comprise as much as several percent of the masses of the planets.

In part because the super-Earths and sub-Neptunes for which we have confirmed masses and radii have orbital periods of $\leq$100 days, i.e., they orbit very close to their host star and are thus subject to atmosphere losses, a strong case can be made that super-Earths are the result of an evolution in which some smaller sub-Neptunes lose their dense hydrogen-rich envelopes (Rogers et al. 2023), leaving the rocky core behind. Escape of the envelopes is thought to be afforded by photoevaporation by extreme X-rays from the nearby star and/or core-powered mass loss facilitated by the intrinsic luminosity of the planet, as well as boil off in which the atmosphere becomes unstable once the protoplanetary disk that confines it dissipates (Ginzburg et al. 2016, Rogers et al. 2023). The result is the well-known radius gap defined by these two classes of planets (Owen &

Wu 2013, Fulton et al. 2017, Gupta & Schlichting 2019). In this view, to first order, the interiors of super-Earths may be similar, if not identical, to those of sub-Neptunes (Bean et al. 2021). This general concept of the evolution of bodies with H_2-rich primary atmospheres to rocky bodies with no such atmospheres has influenced our understanding of how Earth acquired its water, and how it may have engulfed H into its metal core, resulting in the observed density deficit in the core (Young et al. 2023).

Discrete metal cores may not exist in sub-Neptunes and, by corollary, also may not exist in their super-Earth descendants, for at least two reasons. First, thermodynamic simulations of the global equilibration between Fe-rich metal, silicate (represented by $MgSiO_3$), and H_2-rich envelopes show that metal should have significant fractions of H, O, and Si (Schlichting & Young 2022), making them buoyant in the magma oceans. Global equilibrium is possible because with dense overlying envelopes of hydrogen-rich supercritical fluid, cooling times are sufficiently slow that magma oceans can persist for 10^9 years (Ginzburg et al. 2016, Rogers et al. 2024). At the temperatures of several thousand degrees and pressures of several gigapascals that likely typify the surfaces of sub-Neptune magma oceans beneath dense H_2-rich envelopes, the hydrogen concentrations in the metal can be at weight percent levels while Si and O can approach 10 wt% (Schlichting & Young 2022). Revised thermodynamic calculations (Young et al. 2023) that include nonideal mixing of the light elements suggest that density deficits in the metal phase where equilibration occurs at temperatures significantly greater than 3,000 K approach 50%, mainly due to H alloying with Fe (Young et al. 2024). The densities of the iron alloyed with the light elements formed under these conditions are comparable to that of the silicate. Analysis of the maximum sizes of metal droplets against disruption by shear stresses in the magma oceans indicates that the metal droplets that become neutrally buoyant at a level determined by the temperature profile in the magma ocean will become mired in the silicate melt, thus precluding metal-silicate differentiation and resulting instead in a horizon of metal at relatively shallow depths (Young et al. 2024). Similarly, Lichtenberg (2021) concluded that turbulent entrainment of metal droplets is likely simply because of the great depth of the sub-Neptune or super-Earth magma oceans.

As an aside, regardless of the depth of metal in the magma oceans, reactions between metal, silicate, and hydrogen at high temperatures and pressures facilitate formation of water. Dissolution of hydrogen produces water by reactions like

$$3\mathrm{H}_{2,\mathrm{silicate}} + \mathrm{SiO}_{2,\mathrm{silicate}} \rightleftharpoons 2\mathrm{H}_2\mathrm{O}_{\mathrm{silicate}} + \mathrm{Si}_{\mathrm{metal}} + 2\mathrm{H}_{\mathrm{metal}}. \qquad 2.$$

Here water in the silicate is seen to be a by-product of the redox reaction that drives hydrogen into the metal. As a consequence, if a metal phase is present in the interiors of sub-Neptunes, it will facilitate production of endogenous water in the planet (Ikoma & Genda 2006, Kite & Schaefer 2021, Schlichting & Young 2022, Young et al. 2023). Because sub-Neptunes have copious amounts of hydrogen, one expects them to harbor significant amounts of water even where they originally accreted dry.

The second reason that discrete metal cores are unlikely for sub-Neptunes that evolve with magma oceans beneath hydrogen-rich envelopes is the phase equilibria of the $MgSiO_3$-Fe-H_2 system. There is sufficient evidence from ab initio molecular dynamics simulations, as well as experiments, to conclude that it is likely that deep in the interiors of sub-Neptune magma oceans, discrete silicate and iron-rich metal phases do not exist. These constraints include the existence of complete miscibility between molten MgO and Fe at temperatures above 7,000 K and pressures of 60 GPa (Wahl & Militzer 2015, Insixiengmay & Stixrude 2025) and extensive solubility along this binary join at lower temperatures and similar pressures (Badro et al. 2018), complete miscibility

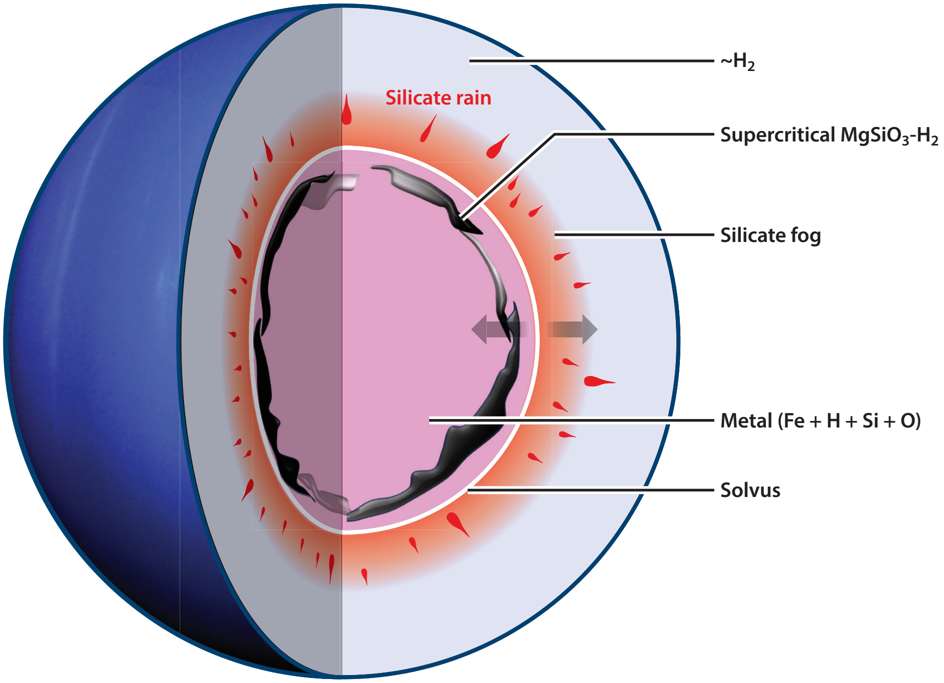

Figure 5

Interpretive diagram representing the structure of a sub-Neptune magma ocean blanket by an H_2-rich envelope. A supercritical silicate-hydrogen magma ocean is present below the silicate-hydrogen solvus, and Fe-rich metal is precluded from forming a discrete core at depth due to suspension of neutrally buoyant droplets in the convecting silicate and/or complete miscibility with silicate. Figure adapted from Young et al. (2024) (CC BY 4.0).

between liquid $MgSiO_3$ and H_2 above about 4,000 K at, for example, 4 GPa (Gilmore & Stixrude 2023), and a pressure-dependent enhancement in the solubility of H in Fe melt relative to silicate melt (Yuan & Steinle-Neumann 2020, Tagawa et al. 2021). In combination, and with the stabilizing effect of a single phase due to entropy of mixing at high temperatures of greater than 5,000 K and pressures of more than 50 GPa in the sub-Neptunes, it is reasonable to conclude that silicate and iron metal are miscible. This proposition awaits further testing.

The picture based on the above analysis for the interior of a sub-Neptune magma ocean blanketed by a hydrogen-rich envelope is shown in **Figure 5**. The figure captures the fact that the magma ocean-envelope interface should be determined by the phase change from supercritical $MgSiO_3$-H_2 to discrete melt and envelope (atmosphere) phases, and that the thermal state of the planet is reflected in the radial position of this binodal surface (also described as the silicate-H_2 solvus). It also shows the suspension of discrete iron-rich metal, if it exists as a discrete phase at all, at relatively shallow depths as a result of reaching a state of neutral buoyancy in the turbulent magma ocean. This structure is an attempt to make use of what we know about the physical chemistry of these silicate-iron-hydrogen systems rather than simply assuming that the core structure is Earth like. Given the significant degeneracies in interpreting mass-radius relationships in subgiant exoplanets, this approach, rooted in physical chemistry, holds promise as a means of escaping our Earth-centric view of sub-Neptunes and super-Earths.

FUTURE ISSUES

1. In order to further constrain planetary core compositions using stable isotope ratios, a database of equilibrium fractionation factors is necessary.
2. Further observations on the core structure of Mars, such as the presence or absence of a solid inner core, will provide strong constraints on the core composition by comparison with phase relations.
3. More experiments on the phase relations of Fe-Si-S and Fe-Si-C alloys at core conditions of Mercury are necessary for precise modeling of the layered structure of Mercury's core.
4. A mission to Venus would be a great way to learn more about its core, given the limited knowledge of its mantle composition.
5. A better understanding of the equilibrium between exoplanetary atmospheres and magma oceans is crucial to understanding the evolution of planets.

DISCLOSURE STATEMENT

The authors are not aware of any affiliations, memberships, funding, or financial holdings that might be perceived as affecting the objectivity of this review.

ACKNOWLEDGMENTS

This review was funded in part by the Alfred P. Sloan Foundation under grant G-202525284. We thank S. Mita for preparing **Figure 2*b*** and calculating the possible range of Earth's core composition.

LITERATURE CITED

Adibekyan V, Dorn C, Sousa SG, Santos NC, Bitsch B, et al. 2021. A compositional link between rocky exoplanets and their host stars. *Science* 374(6565):330–32

Agol E, Dorn C, Grimm SL, Turbet M, Ducrot E, et al. 2021. Refining the transit-timing and photometric analysis of TRAPPIST-1: masses, radii, densities, dynamics, and ephemerides. *Planet. Sci. J.* 2(1):1

Allègre C, Manhès G, Lewin E. 2001. Chemical composition of the Earth and the volatility control on planetary genetics. *Earth Planet. Sci. Lett.* 185:49–69

Anders E, Grevesse N. 1989. Abundances of the elements: meteoritic and solar. *Geochim. Cosmochim. Acta* 53:197–214

Andrault D, Bolfan-Casanova N, Nigro GL, Bouhifd MA, Garbarino G, et al. 2011. Solidus and liquidus profiles of chondritic mantle: implication for melting of the Earth across its history. *Earth Planet. Sci. Lett.* 304:251–59

Antonangeli D, Krisch M, Requardt H, Mermet A, Farber D, et al. 2012. Simultaneous sound velocity and density measurements of hcp iron up to 93 GPa and 1100 K: an experimental test of the Birch's law at high temperature. *Earth Planet. Sci. Lett.* 331:210–14

Anzellini S, Dewaele A, Mezouar M, Loubeyre P, Morard G. 2013. Melting of iron at Earth's inner core boundary based on fast X-ray diffraction. *Science* 340:464–66

Arveson SM, Deng J, Karki BB, Lee KKM. 2019. Evidence for Fe-Si-O liquid immiscibility at deep Earth pressures. *PNAS* 116(21):10238–43

Badro J, Aubert J, Hirose K, Nomura R, Blanchard I, et al. 2018. Magnesium partitioning between Earth's mantle and core and its potential to drive an early exsolution geodynamo. *Geophys. Res. Lett.* 45(24):13240–48

Badro J, Côté AS, Brodholt JP. 2014. A seismologically consistent compositional model of Earth's core. *PNAS* 111(21):7542–45

Badro J, Fiquet G, Guyot F, Gregoryanz E, Occelli F, et al. 2007. Effect of light elements on the sound velocities in solid iron: implications for the composition of Earth's core. *Earth Planet. Sci. Lett.* 254:233–38

Bean JL, Raymond SN, Owen JE. 2021. The nature and origins of sub-Neptune size planets. *J. Geophys. Res. Planets* 126(1):e06639

Bigeleisen J, Mayer MG. 1947. *Calculation of equilibrium constants for isotopic exchange reactions*. Rep. MDDC-707, Atomic Energy Commission

Birch F. 1952. Elasticity and constitution of the Earth's interior. *J. Geophys. Res.* 57(2):227–86

Bonnand P, Williams H, Parkinson I, Wood B, Halliday A. 2016. Stable chromium isotopic composition of meteorites and metal–silicate experiments: implications for fractionation during core formation. *Earth Planet. Sci. Lett.* 435:14–21

Boukaré C-E, Ricard Y, Fiquet G. 2015. Thermodynamics of the MgO–FeO–SiO_2 system up to 140 GPa: application to the crystallization of Earth's magma ocean. *J. Geophys. Res. Solid Earth* 120(9):6085–101

Brennan MC, Fischer RA, Irving JCE. 2020. Core formation and geophysical properties of Mars. *Earth Planet. Sci. Lett.* 530:115923

Bridgestock LJ, Williams H, Rehkmper M, Larner F, Giscard MD, et al. 2014. Unlocking the zinc isotope systematics of iron meteorites. *Earth Planet. Sci. Lett.* 400:153–64

Chabot NL, Wollack EA, Klima RL, Minitti ME. 2014. Experimental constraints on Mercury's core composition. *Earth Planet. Sci. Lett.* 390:199–208

Chen B, Li J, Hauck SA. 2008. Non-ideal liquidus curve in the Fe-S system and Mercury's snowing core. *Geophys. Res. Lett.* 35(7):2008GL033311

Christensen UR. 2006. A deep dynamo generating Mercury's magnetic field. *Nature* 444(7122):1056–58

Corgne A, Keshav S, Wood BJ, McDonough WF, Fei Y. 2008. Metal–silicate partitioning and constraints on core composition and oxygen fugacity during Earth accretion. *Geochim. Cosmochim. Acta* 72(2):574–89

Dalou C, Fri E, Deligny C, Piani L, Caumon MC, et al. 2019. Redox control on nitrogen isotope fractionation during planetary core formation. *PNAS* 116(29):14485–94

Dauphas N, Poitrasson F, Burkhardt C, Kobayashi H, Kurosawa K. 2015. Planetary and meteoritic Mg/Si and δ^{30}Si variations inherited from solar nebula chemistry. *Earth Planet. Sci. Lett.* 427:236–48

de Kleer K, Cambioni S, Shepard M. 2021. The surface of (16) Psyche from thermal emission and polarization mapping. *Planet. Sci. J.* 2(4):149

Decremps F, Antonangeli D, Gauthier M, Ayrinhac S, Morand M, et al. 2014. Sound velocity of iron up to 152 GPa by picosecond acoustics in diamond anvil cell. *Geophys. Res. Lett.* 41(5):1459–64

Dibb SD, Bell JF, Elkins-Tanton LT, Williams DA. 2023. Visible to near-infrared reflectance spectroscopy of asteroid (16) Psyche: implications for the Psyche mission's science investigations. *Earth Space Sci.* 10(1):e2022EA002694

Doyle AE, Young ED, Klein B, Zuckerman B, Schlichting HE. 2019. Oxygen fugacities of extrasolar rocks: evidence for an Earth-like geochemistry of exoplanets. *Science* 366(6463):356–59

Dreibus G, Palme H. 1996. Cosmochemical constraints on the sulfur content in the Earth's core. *Geochim. Cosmochim. Acta* 60(7):1125–30

Drilleau M, Samuel H, Garcia RF, Rivoldini A, Perrin C, et al. 2022. Marsquake locations and 1-D seismic models for Mars from insight data. *J. Geophys. Res. Planets* 127(9):e2021JE007067

Durán C, Khan A, Ceylan S, Zenhäusern G, Stähler S, et al. 2022. Seismology on Mars: an analysis of direct, reflected, and converted seismic body waves with implications for interior structure. *Phys. Earth Planet. Inter.* 325:106851

Dziewonski AM, Anderson DL. 1981. Preliminary reference Earth model. *Phys. Earth Planet. Inter.* 25(4):297–356

Edmund E, Gauthier M, Antonangeli D, Ayrinhac S, Boccato S, et al. 2020. Picosecond acoustics technique to measure the sound velocities of Fe-Si alloys and Si single-crystals at high pressure. *Minerals* 10(3):214

Edmund E, Morard G, Baron MA, Rivoldini A, Yokoo S, et al. 2022. The Fe-FeSi phase diagram at Mercury's core conditions. *Nat. Commun.* 13(1):387

Elardo SM, Shahar A, Mock TD, Sio CK. 2019. The effect of core composition on iron isotope fractionation between planetary cores and mantles. *Earth Planet. Sci. Lett.* 513:124–34

Elkins-Tanton LT, Asphaug E, Bell JF, Bercovici H, Bills B, et al. 2020. Observations, meteorites, and models: a preflight assessment of the composition and formation of (16) Psyche. *J. Geophys. Res. Planets* 125(3):e2019JE006296

Elkins-Tanton LT, Zuber MT, Banfield D, Bell JF, Brodsky JL, et al. 2022. Distinguishing the origin of asteroid (16) Psyche. *Space Sci. Rev.* 218(2):17

Farihi J, Jura M, Lee JE, Zuckerman B. 2010. Strengthening the case for asteroidal accretion: evidence for subtle and diverse disks at white dwarfs. *Astrophys. J.* 714(2):1386–97

Farnocchia D, Fuentes-Muñoz O, Park RS, Baer J, Chesley SR. 2024. Mass, density, and radius of asteroid (16) Psyche from high-precision astrometry. *Astronom. J.* 168(1):21

Fei Y, Li J, Bertka CM, Prewitt CT. 2000. Structure type and bulk modulus of Fe_3S, a new iron-sulfur compound. *Am. Mineral.* 85(11–12):1830–33

Fiquet G, Irifune T, Fei Y, Prakapenka V, Tomioka N, et al. 2010. Melting of peridotite to 140 gigapascals. *Science* 329:1516–18

Fischer RA, McDonough WF. 2024. *Earth's Core Composition and Core Formation*, Vol. 1. Elsevier

Fischer RA, Nakajima Y, Campbell AJ, Frost DJ, Harries D, et al. 2015. High pressure metal–silicate partitioning of Ni, Co, V, Cr, Si, and O. *Geochim. Cosmochim. Acta* 167:177–94

Fischer-Gödde M, Kleine T. 2017. Ruthenium isotopic evidence for an inner Solar System origin of the late veneer. *Nature* 541(7638):525–27

Fressin F, Torres G, Charbonneau D, Bryson ST, Christiansen J, et al. 2013. The false positive rate of Kepler and the occurrence of planets. *Astrophys. J.* 766:81

Fulton BJ, Petigura EA, Howard AW, Isaacson H, Marcy GW, et al. 2017. The California-Kepler Survey. III. A gap in the radius distribution of small planets. *Astronom. J.* 154:109

Gänsicke BT, Koester D, Farihi J, Girven J, Parsons SG, Breedt E. 2012. The chemical diversity of exo-terrestrial planetary debris around white dwarfs. *MNRAS* 424(1):333–47

Geballe ZM, Jeanloz R. 2014. Solid phases of FeSi to 47 GPa and 2800 K: new data. *Am. Mineral.* 99(4):720–23

Genova A, Goossens S, Mazarico E, Lemoine FG, Neumann GA, et al. 2019. Geodetic evidence that Mercury has a solid inner core. *Geophys. Res. Lett.* 46(7):3625–33

Gilmore T, Stixrude LP. 2023. Mixing of rocky cores and hydrogen envelopes from terrestrial to sub-Neptune planets. *AGU Fall Meet. Abstr.* 2023:MR24A-06

Ginzburg S, Schlichting HE, Sari R. 2016. Super-Earth atmospheres: self-consistent gas accretion and retention. *Astrophys. J.* 825:29

Gomi H, Hirose K. 2023. Impurity resistivity of the Earth's inner core. *J. Geophys. Res. Solid Earth* 128:e2023JB027097

Gomi H, Hirose K. 2025. Strong compositional gradient in the Earth's inner core? *Phys. Earth Planet. Inter.* 362:107349

Gupta A, Schlichting HE. 2019. Sculpting the valley in the radius distribution of small exoplanets as a by-product of planet formation: the core-powered mass-loss mechanism. *MNRAS* 487(1):24–33

Hasegawa M, Hirose K, Oka K, Ohishi Y. 2021. Liquidus phase relations and solid-liquid partitioning in the Fe-Si-C system under core pressures. *Geophys. Res. Lett.* 48:e2021GL092681

Hauck SA, Margot J, Solomon SC, Phillips RJ, Johnson CL, et al. 2013. The curious case of Mercury's internal structure. *J. Geophys. Res. Planets* 118(6):1204–20

Helffrich G, Hirose K, Nomura R. 2020. Thermodynamical modeling of liquid Fe-Si-Mg-O: molten magnesium silicate release from the core. *Geophys. Res. Lett.* 47:e2020GL089218

Helled R, Stevenson DJ. 2024. The fuzzy cores of Jupiter and Saturn. *AGU Adv.* 5:e2024AV001171

Hikosaka K, Tagawa S, Hirose K, Okuda Y, Oka K, et al. 2022. Melting phase relations in Fe–Si–H at high pressure and implications for Earth's inner core crystallization. *Sci. Rep.* 12:10000

Hin RC, Burkhardt C, Schmidt MW, Bourdon B, Kleine T. 2013. Experimental evidence for Mo isotope fractionation between metal and silicate liquids. *Earth Planet. Sci. Lett.* 379:38–48

Hin RC, Fitoussi C, Schmidt MW, Bourdon B. 2014. Experimental determination of the Si isotope fractionation factor between liquid metal and liquid silicate. *Earth Planet. Sci. Lett.* 387:55–66

Hin RC, Schmidt MW, Bourdon B. 2012. Experimental evidence for the absence of iron isotope fractionation between metal and silicate liquids at 1 GPa and 1250–1300 C and its cosmochemical consequences. *Geochim. Cosmochim. Acta* 93:164–81

Hinkel NR, Timmes F, Young PA, Pagano MD, Turnbull MC. 2014. Stellar abundances in the solar neighborhood: the Hypatia Catalog. *Astronom. J.* 148(3):54

Hinkel NR, Young ED. 2025. Abundances of elements in solar systems. In *Treatise on Geochemistry*, ed. A Anbar, D Weis. Elsevier. 3rd ed.

Hirose K, Morard G, Sinmyo R, Umemoto K, Hernlund J, et al. 2017. Crystallization of silicon dioxide and compositional evolution of the Earth's core. *Nature* 543(7643):99–102

Hirose K, Tagawa S, Kuwayama Y, Sinmyo R, Morard G, et al. 2019. Hydrogen limits carbon in liquid iron. *Geophys. Res. Lett.* 46:5190–97

Hirose K, Wood B, Vočadlo L. 2021. Light elements in the Earth's core. *Nat. Rev. Earth Environ.* 2(9):645–58

Huang D, Li Y, Khan A, Sossi P, Giardini D, Murakami M. 2023. Thermoelastic properties of liquid Fe-rich alloys under Martian core conditions. *Geophys. Res. Lett.* 50(6):e2022GL102271

Huang H, Fan L, Liu X, Xu F, Wu Y, et al. 2022. Inner core composition paradox revealed by sound velocities of Fe and Fe-Si alloy. *Nat. Commun.* 13(1):616

Huang H, Leng C, Wang Q, Yang G, Hu X, et al. 2018. Measurements of sound velocity of liquid Fe-11.8 wt % S up to 211.4 GPa and 6,150 K. *J. Geophys. Res. Solid Earth* 123:4730–39

Ikoma M, Genda H. 2006. Constraints on the mass of a habitable planet with water of nebular origin. *Astrophys. J.* 648:696–706

Insixiengmay L, Stixrude L. 2025. MgO miscibility in liquid iron. *Earth Planet. Sci. Lett.* 654:119242

Irving JCE, Lekić V, Durán C, Drilleau M, Kim D, et al. 2023. First observations of core-transiting seismic phases on Mars. *PNAS* 120(18):e2217090120

Jura M, Farihi J, Zuckerman B. 2007. Externally polluted white dwarfs with dust disks. *Astrophys. J.* 663(2):1285–90

Jura M, Young E. 2014. Extrasolar cosmochemistry. *Annu. Rev. Earth Planet. Sci.* 42:45–67

Kawaguchi SI, Morard G, Kuwayama Y, Hirose K, Hirao N, Ohishi Y. 2022. Density determination of liquid iron-nickel-sulfur at high pressure. *Am. Mineral.* 107(7):1254–61

Kempl J, Vroon P, Zinngrebe E, van Westrenen W. 2013. Si isotope fractionation between Si-poor metal and silicate melt at pressure–temperature conditions relevant to metal segregation in small planetary bodies. *Earth Planet. Sci. Lett.* 368:61–68

Khan A, Huang D, Durán C, Sossi PA, Giardini D, Murakami M. 2023. Evidence for a liquid silicate layer atop the Martian core. *Nature* 622(7984):718–23

Kim T, Ko B, Greenberg E, Prakapenka V, Shim S, et al. 2020. Low melting temperature of anhydrous mantle materials at the core-mantle boundary. *Geophys. Res. Lett.* 47(20):e2020GL089345

Kite ES, Fegley B Jr., Schaefer L, Ford EB. 2019. Superabundance of exoplanet sub-Neptunes explained by fugacity crisis. *Astrophys. J. Lett.* 887(2):L33

Kite ES, Schaefer L. 2021. Water on hot rocky exoplanets. *Astrophys. J. Lett.* 909:L22

Komabayashi T. 2014. Thermodynamics of melting relations in the system Fe–FeO at high pressure: implications for oxygen in the Earth's core. *J. Geophys. Res. Solid Earth* 119(5):4164–77

Kuwayama Y, Hirose K. 2004. Phase relations in the system Fe-FeSi at 21 GPa. *Am. Mineral.* 89:273–76

Kuwayama Y, Morard G, Nakajima Y, Hirose K, Baron AQR, et al. 2020. Equation of state of liquid iron under extreme conditions. *Phys. Rev. Lett.* 124(16):165701

Labidi J, Shahar A, Le Losq C, Hillgren V, Mysen B, Farquhar J. 2016. Experimentally determined sulfur isotope fractionation between metal and silicate and implications for planetary differentiation. *Geochim. Cosmochim. Acta* 175:181–94

Lark LH, Head JW, Huber C. 2023. Evidence for a carbon-rich Mercury from the distribution of low-reflectance material (LRM) associated with large impact basins. *Earth Planet. Sci. Lett.* 613:118192

Lazar C, Young ED, Manning CE. 2012. Experimental determination of equilibrium nickel isotope fractionation between metal and silicate from 500°C to 950°C. *Geochim. Cosmochim. Acta* 86:276–95

Le Maistre S, Rivoldini A, Caldiero A, Yseboodt M, Baland RM, et al. 2023. Spin state and deep interior structure of Mars from insight radio tracking. *Nature* 619(7971):733–37

Li Y, Dasgupta R, Tsuno K. 2015. The effects of sulfur, silicon, water, and oxygen fugacity on carbon solubility and partitioning in Fe-rich alloy and silicate melt systems at 3 GPa and 1600°C: implications for core–mantle differentiation and degassing of magma oceans and reduced planetary mantles. *Earth Planet. Sci. Lett.* 415:54–66

Li Y, Vočadlo L, Brodholt JP. 2018. The elastic properties of hcp-Fe alloys under the conditions of the Earth's inner core. *Earth Planet. Sci. Lett.* 493:118–27
Li YF, Marty B, Shcheka S, Zimmermann L, Keppler H. 2016. Nitrogen isotope fractionation during terrestrial core-mantle separation. *Geochem. Perspect. Lett.* 2:138–47
Lichtenberg T. 2021. Redox hysteresis of super-Earth exoplanets from magma ocean circulation. *Astrophys. J. Lett.* 914(1):L4
Malavergne V, Toplis MJ, Berthet S, Jones J. 2010. Highly reducing conditions during core formation on Mercury: implications for internal structure and the origin of a magnetic field. *Icarus* 206(1):199–209
Man L, Li X, Boffa Ballaran T, Zhou W, Chantel J, et al. 2025. The structure and stability of $Fe_{4+x}S_3$ and its potential to form a Martian inner core. *Nat. Commun.* 16(1):1710
Manser CJ, Gänsicke BT, Eggl S, Hollands M, Izquierdo P, et al. 2019. A planetesimal orbiting within the debris disc around a white dwarf star. *Science* 364(6435):66–69
Mao H, Wang J, Lin J, Zhang J, Hazen R. 2012. Sound velocities of Fe and Fe-Si alloy in the Earth's core. *PNAS* 109(45):18070–75
Margot JL, Campbell DB, Giorgini JD, Jao JS, Snedeker LG, et al. 2021. Spin state and moment of inertia of Venus. *Nat. Astron.* 5(7):676–83
Margot JL, Peale SJ, Jurgens RF, Slade MA, Holin IV. 2007. Large longitude libration of Mercury reveals a molten core. *Science* 316(5825):710–14
Mashino I, Miozzi F, Hirose K, Morard G, Sinmyo R, et al. 2019. Melting experiments on the Fe-C binary system up to 255 GPa: constraints on the carbon content in the Earth's core. *Earth Planet. Sci. Lett.* 515:135–44
Militzer B, Hubbard WB, Wahl S, Lunine JI, Galanti E, et al. 2022. Juno spacecraft measurements of Jupiter's gravity imply a dilute core. *Planet. Sci. J.* 3(8):185
Miozzi F, Morard G, Antonangeli D, Baron MA, Boccato S, et al. 2020. Eutectic melting of Fe-3 at% Si-4 at% C up to 200 GPa and implications for the Earth's core. *Earth Planet. Sci. Lett.* 544:116382
Mita S, Tagawa S, Hirose K, Ikuta N. 2025. Fe-FeH eutectic melting curve and the estimates of Earth's core temperature and composition. *J. Geophys. Res. Solid Earth* 130(1):e2024JB029283
Mizuno H. 1980. Formation of the giant planets. *Prog. Theor. Phys.* 64:544–57
Montagner JP, Kennett BLN. 1996. How to reconcile body-wave and normal-mode reference Earth models. *Geophys. J. Int.* 125:229–48
Morard G, Katsura T. 2010. Pressure–temperature cartography of Fe–S–Si immiscible system. *Geochim. Cosmochim. Acta* 74(12):3659–67
Morard G, Siebert J, Andraut D, Guignot N, Garbarino G, et al. 2013. The Earth's core composition from high pressure density measurements of liquid iron alloys. *Earth Planet. Sci. Lett.* 373:169–78
Morard G, Siebert J, Badro J. 2014. Partitioning of Si and platinum group elements between liquid and solid Fe–Si alloys. *Geochim. Cosmochim. Acta* 132:94–100
Ni P, Zhang Y, Mao HK, Xiao Y, Lin JF, Shahar A. 2022. Planet size controls Fe isotope fractionation between mantle and core. *Geophys. Res. Lett.* 49(17):e2022GL098451
Nittler LR, Starr RD, Weider SZ, McCoy TJ, Boynton WV, et al. 2011. The major-element composition of Mercury's surface from MESSENGER X-ray spectrometry. *Science* 333(6051):1847–50
Nomura R, Ozawa H, Tateno S, Hirose K, Hernlund J, et al. 2014. Low core-mantle boundary temperature inferred from the solidus of pyrolite. *Science* 343(6176):1234–37
Oka K, Ikuta N, Tagawa S, Hirose K, Ohishi Y. 2022. Melting experiments on Fe-O-H and Fe-H: evidence for eutectic melting in Fe-FeH and implications for hydrogen in the core. *Geophys. Res. Lett.* 49:e2022GL099420
O'Neill C. 2021. End-member Venusian core scenarios: Does Venus have an inner core? *Geophys. Res. Lett.* 48(17):e2021GL095499
O'Neill HSC, Canil D, Rubie DC. 1998. Oxide–metal equilibria to 2500°C and 25 GPa: implications for core formation and the light component in the Earth's core. *J. Geophys. Res.* 103(B6):12239–60
Owen JE, Wu Y. 2013. Kepler planets: a tale of evaporation. *Astrophys. J.* 775:105
Pamato MG, Li Y, Antonangeli D, Miozzi F, Morard G, et al. 2020. Equation of state of *hcp* Fe-C-Si alloys and the effect of C incorporation mechanism on the density of *hcp* Fe alloys at 300 K. *J. Geophys. Res. Solid Earth* 125(12):e2020JB020159

Peplowski PN, Klima RL, Lawrence DJ, Ernst CM, Denevi BW, et al. 2016. Remote sensing evidence for an ancient carbon-bearing crust on Mercury. *Nat. Geosci.* 9(4):273–76

Petricca F, Castillo-Rogez JC, Genova A, Melwani Daswani M, Styczinski MJ, et al. 2025. Partial differentiation of Europa and implications for the origin of materials in the Jupiter system. *Nat. Astron.* 9(4):501–11

Poirier JP. 1994. Light elements in the Earth's outer core: a critical review. *Phys. Earth Planet. Inter.* 85:319–37

Rai N, Van Westrenen W. 2013. Core-mantle differentiation in Mars. *J. Geophys. Res. Planets* 118(6):1195–203

Righter K, Chabot NL. 2011. Moderately and slightly siderophile element constraints on the depth and extent of melting in early Mars. *Meteorit. Planet. Sci.* 46(2):157–76

Rivoldini A, Van Hoolst T. 2013. The interior structure of Mercury constrained by the low-degree gravity field and the rotation of Mercury. *Earth Planet. Sci. Lett.* 377–378:62–72

Rogers JG, Owen JE, Schlichting HE. 2024. Under the light of a new star: evolution of planetary atmospheres through protoplanetary disc dispersal and boil-off. *MNRAS* 529(3):2716–33

Rogers JG, Schlichting HE, Owen JE. 2023. Conclusive evidence for a population of water worlds around M dwarfs remains elusive. *Astrophys. J. Lett.* 947(1):L19

Rose-Weston L, Brenan JM, Fei Y, Secco RA, Frost DJ. 2009. Effect of pressure, temperature, and oxygen fugacity on the metal-silicate partitioning of Te, Se, and S: implications for Earth differentiation. *Geochim. Cosmochim. Acta* 73(15):4598–615

Roskosz M, Luais B, Watson HC, Toplis MJ, Alexander CM, Mysen BO. 2006. Experimental quantification of the fractionation of Fe isotopes during metal segregation from a silicate melt. *Earth Planet. Sci. Lett.* 248(3–4):851–67

Sakai F, Hirose K, Morard G. 2023. Partitioning of silicon and sulfur between solid and liquid iron under core pressures: constraints on Earth's core composition. *Earth Planet. Sci. Lett.* 624:118449

Sakai F, Hirose K, Umemoto K. 2022. Melting experiments on Fe-C-O to 200 GPa: liquidus phase constraints on core composition. *Geochem. Perspect. Lett.* 22:1–4

Sakamaki T, Ohtani E, Fukui H, Kamada S, Takahashi S, et al. 2016. Constraints on Earth's inner core composition inferred from measurements of the sound velocity of hcp-iron in extreme conditions. *Sci. Adv.* 2:e1500802

Samuel H, Drilleau M, Rivoldini A, Xu Z, Huang Q, et al. 2023. Geophysical evidence for an enriched molten silicate layer above Mars's core. *Nature* 622(7984):712–17

Sanloup C, Fei Y. 2004. Closure of the Fe–S–Si liquid miscibility gap at high pressure. *Phys. Earth Planet. Inter.* 147(1):57–65

Savage PS, Moynier F, Chen H, Shofner G, Siebert J, et al. 2015. Copper isotope evidence for large-scale sulphide fractionation during Earth's differentiation. *Geochem. Perspect. Lett.* 1(1):53–64

Schauble EA. 2004. Applying stable isotope fractionation theory to new systems. *Rev. Mineral. Geochem.* 55(1):65–111

Schlichting HE, Young ED. 2022. Chemical equilibrium between cores, mantles, and atmospheres of super-Earths and sub-Neptunes, and implications for their compositions, interiors and evolution. *Planet. Sci. J.* 3(5):127

Schubert G, Sohl F, Hussmann H. 2009. Interiors of Europa. In *Europa*, ed. RT Pappalardo, WB McKinnon, KK Khurana. University of Arizona Press

Schuessler JA, Schoenberg R, Behrens H, von Blanckenburg F. 2007. The experimental calibration of the iron isotope fractionation factor between pyrrhotite and peralkaline rhyolitic melt. *Geochim. Cosmochim. Acta* 71(2):417–33

Scott ERD. 2020. Iron meteorites: composition, age, and origin. In *Oxford Research Encyclopedia of Planetary Science*. Oxford University Press

Seo C, Ito Y, Fujii Y. 2024. Role of magma oceans in controlling carbon and oxygen of sub-Neptune atmospheres. *Astrophys. J.* 975(1):14

Shah O, Helled R, Alibert Y, Mezger K. 2022. Possible chemical composition and interior structure models of Venus inferred from numerical modelling. *Astrophys. J.* 926(2):217

Shahar A, Elardo SM, Macris CA. 2017. Equilibrium fractionation of non-traditional stable isotopes: an experimental perspective. *Rev. Mineral. Geochem.* 82(1):65–83

Shahar A, Hillgren VJ, Young ED, Fei Y, Macris CA, Deng L. 2011. High-temperature Si isotope fractionation between iron metal and silicate. *Geochim. Cosmochim. Acta* 75(23):7688–97

Shahar A, Schauble EA, Caracas R, Gleason AE, Reagan MM, et al. 2016. Pressure-dependent isotopic composition of iron alloys. *Science* 352(6285):580–82

Shahar A, Young ED. 2020. Astrophysical insight from iron isotope fractionation during planetary differentiation. *Philos. Trans. R. Soc. A* 378(2187):20200172

Shahar A, Young ED, Manning CE. 2008. Equilibrium high-temperature Fe isotope fractionation between fayalite and magnetite: an experimental calibration. *Earth Planet. Sci. Lett.* 268(3–4):330–38

Shahar A, Ziegler K, Young ED, Ricolleau A, Schauble EA, Fei Y. 2009. Experimentally determined Si isotope fractionation between silicate and Fe metal and implications for Earth's core formation. *Earth Planet. Sci. Lett.* 288(1–2):228–34

Smith DE, Zuber MT, Phillips RJ, Solomon SC, Hauck SA, et al. 2012. Gravity field and internal structure of Mercury from MESSENGER. *Science* 336(6078):214–17

Smrekar SE, Davaille A, Sotin C. 2018. Venus interior structure and dynamics. *Space Sci. Rev.* 214(5):88

Soderlund KM, Stanley S, Cao H, Calkins MA, Browning MK. 2025. Puzzles in planetary dynamos: implications for planetary interiors. *Annu. Rev. Earth Planet. Sci.* 53:305–37

Stähler SC, Khan A, Banerdt WB, Lognonné P, Giardini D, et al. 2021. Seismic detection of the Martian core. *Science* 373(6553):443–48

Steenstra ES, Van Westrenen W. 2018. A synthesis of geochemical constraints on the inventory of light elements in the core of Mars. *Icarus* 315:69–78

Steenstra ES, Van Westrenen W. 2020. Geochemical constraints on core-mantle differentiation in Mercury and the aubrite parent body. *Icarus* 340:113621

Stewart AJ, Schmidt MW, Van Westrenen W, Liebske C. 2007. Mars: a new core-crystallization regime. *Science* 316(5829):1323–25

Tagawa S, Sakamoto N, Hirose K, Yokoo S, Hernlund J, et al. 2021. Experimental evidence for hydrogen incorporation into Earth's core. *Nat. Commun.* 12(1):2588

Takahashi S, Ohtani E, Terasaki H, Ito Y, Shibazaki Y, et al. 2013. Phase relations in the carbon-saturated C–Mg–Fe–Si–O system and C and Si solubility in liquid Fe at high pressure and temperature: implications for planetary interiors. *Phys. Chem. Miner.* 40(8):647–57

Tao R, Fei Y. 2021. High-pressure experimental constraints of partitioning behavior of Si and S at the Mercury's inner core boundary. *Earth Planet. Sci. Lett.* 562:116849

Tateno S, Hirose K, Sinmyo R, Morard G, Hirao N, et al. 2018. Melting of Fe–Si–S alloys to core pressures: silicon in the core? *Am. Mineral.* 103:742–48

Thibault Y, Walter MJ. 1995. The influence of pressure and temperature on the metal–silicate partition coefficients of nickel and cobalt in a model C1 chondrite and implications for metal segregation in a deep magma ocean. *Geochim. Cosmochim. Acta* 59:991–1002

Thompson S, Sugimura-Komabayashi E, Komabayashi T, McGuire C, Breton H, et al. 2022. High-pressure melting experiments of Fe_3S and a thermodynamic model of the Fe–S liquids for the Earth's core. *J. Phys. Condens. Matter* 34:394003

Trierweiler IL, Doyle AE, Young ED. 2023. A chondritic solar neighborhood. *Planet. Sci. J.* 4(8):136

Trønnes RG, Baron MA, Eigenmann KR, Guren MG, Heyn BH, et al. 2019. Core formation, mantle differentiation and core-mantle interaction within Earth and the terrestrial planets. *Tectonophysics* 760:165–98

Tsuno K, Frost DJ, Rubie DC. 2011. The effects of nickel and sulphur on the core–mantle partitioning of oxygen in Earth and Mars. *Phys. Earth Planet. Inter.* 185(1–2):1–12

Tsuno K, Grewal DS, Dasgupta R. 2018. Core-mantle fractionation of carbon in Earth and Mars: the effects of sulfur. *Geochim. Cosmochim. Acta* 238:477–95

Tsuno K, Ohtani E. 2009. Eutectic temperatures and melting relations in the Fe–O–S system at high pressures and temperatures. *Phys. Chem. Miner.* 36(1):9–17

Umemoto K, Hirose K. 2020. Chemical compositions of the outer core examined by first principles calculations. *Earth Planet. Sci. Lett.* 531:116009

Unterborn CT, Desch SJ, Haldemann J, Lorenzo A, Schulze JG, et al. 2023. The nominal ranges of rocky planet masses, radii, surface gravities, and bulk densities. *Astrophys. J.* 944(1):42

Urey HC. 1947. The thermodynamic properties of isotopic substances. *J. Chem. Soc.* 1947:562–81

Vander Kaaden KE, McCubbin FM. 2015. Exotic crust formation on Mercury: consequences of a shallow, FeO-poor mantle. *J. Geophys. Res. Planets* 120(2):195–209

Vander Kaaden KE, McCubbin FM, Turner AA, Ross DK. 2020. Constraints on the abundances of carbon and silicon in Mercury's core from experiments in the Fe-Si-C system. *J. Geophys. Res. Planets* 125(5):e2019JE006239

Vočadlo L, Alfè D, Gillan MJ, Price GD. 2003. The properties of iron under core conditions from first principles calculations. *Phys. Earth Planet. Inter.* 140:101–25

Wahl SM, Militzer B. 2015. High-temperature miscibility of iron and rock during terrestrial planet formation. *Earth Planet. Sci. Lett.* 410:25–33

Wakamatsu T, Ohta K, Tagawa S, Yagi T, Hirose K, et al. 2022. Compressional wave velocity for iron hydrides to 100 gigapascals via picosecond acoustics. *Phys. Chem. Miner.* 49:17

Wang W, Li Y, Brodholt JP, Vočadlo L, Walter MJ, et al. 2021. Strong shear softening induced by superionic hydrogen in Earth's inner core. *Earth Planet. Sci. Lett.* 568:117014

Wiechert E. 1897. Ueber die massenverteilung im inneren der erde. *Nachr. Ges. Wiss. Gtt. Math.-Phys. Kl.* 1897:221–43

Williams HM, McCammon CA, Peslier AH, Halliday AN, Teutsch N, et al. 2004. Iron isotope fractionation and the oxygen fugacity of the mantle. *Science* 304(5677):1656–59

Xu R, Xiao Z, Wang Y, Cui J. 2024. Less than one weight percent of graphite on the surface of Mercury. *Nat. Astron.* 8(3):280–89

Xu Y, Lin Y, Wu P, Namur O, Zhang Y, Charlier B. 2024. A diamond-bearing core-mantle boundary on Mercury. *Nat. Commun.* 15(1):5061

Yoder CF, Konopliv AS, Yuan DN, Standish EM, Folkner WM. 2003. Fluid core size of Mars from detection of the solar tide. *Science* 300(5617):299–303

Yokoo S, Edmund E, Morard G, Baron MA, Boccato S, et al. 2023. Composition-dependent thermal equation of state of B2 Fe-Si alloys at high pressure. *Am. Mineral.* 108(3):536–42

Yokoo S, Hirose K. 2024. Melting experiments on Fe-S-O-C alloys at Martian core conditions: possible structures in the O- and C-bearing core of Mars. *Geochim. Cosmochim. Acta* 378:234–44

Yokoo S, Hirose K, Sinmyo R, Tagawa S. 2019. Melting experiments on liquidus phase relations in the Fe-S-O ternary system under core pressures. *Geophys. Res. Lett.* 46:5137–45

Yokoo S, Hirose K, Tagawa S, Morard G, Ohishi Y. 2022. Stratification in planetary cores by liquid immiscibility in Fe-S-H. *Nat. Commun.* 13(1):644

Yokoo S, Umemoto K, Hirose K. 2024. Equation of state of liquid Fe_7C_3 and thermodynamic modeling of the liquidus phase relations in the Fe-C system. *J. Geophys. Res. Solid Earth* 129(3):e2023JB028116

Yoshizaki T, McDonough WF. 2020. The composition of Mars. *Geochim. Cosmochim. Acta* 273:137–62

Young ED, Manning CE, Schauble EA, Shahar A, Macris CA, et al. 2015. High-temperature equilibrium isotope fractionation of non-traditional stable isotopes: experiments, theory, and applications. *Chem. Geol.* 395:176–95

Young ED, Shahar A, Schlichting HE. 2023. Earth shaped by primordial H_2 atmospheres. *Nature* 616(7956):306–11

Young ED, Stixrude L, Rogers JG, Schlichting HE, Marcum SP. 2024. Phase equilibria of sub-Neptunes and super-Earths. *Planet. Sci. J.* 5(12):268

Yuan L, Steinle-Neumann G. 2020. Strong sequestration of hydrogen into the Earth's core during planetary differentiation. *Geophys. Res. Lett.* 47(15):e2020GL088303

Zeng L, Jacobsen SB, Sasselov DD, Petaev MI, Vanderburg A, et al. 2019. Growth model interpretation of planet size distribution. *PNAS* 116(20):9723–28

Zuckerman B, Koester D, Melis C, Hansen BM, Jura M. 2007. The chemical composition of an extrasolar minor planet. *Astrophys. J.* 671(1):872

Zuckerman B, Young ED. 2018. Characterizing the chemistry of planetary materials around white dwarf stars. In *Handbook of Exoplanets*, ed. JA Belmonte, H Deeg. Springer International Publishing